NOAA Technical Memorandum NMFS-AFSC-475

# A Flexible Approach for Processing Data Collected Using Trawl-Mounted CTDs During Alaska Bottom-Trawl Surveys

S. K. Rohan, N. E. Charriere, B. Riggle, C. A. O'Leary, and N. W. Raring

September 2023

U.S. DEPARTMENT OF COMMERCE

National Oceanic and Atmospheric Administration
National Marine Fisheries Service
Alaska Fisheries Science Center

The National Marine Fisheries Service's Alaska Fisheries Science Center uses the NOAA Technical Memorandum series to issue informal scientific and technical publications when complete formal review and editorial processing are not appropriate or feasible. Documents within this series reflect sound professional work and may be referenced in the formal scientific and technical literature.

The NMFS-AFSC Technical Memorandum series of the Alaska Fisheries Science Center continues the NMFS-F/NWC series established in 1970 by the Northwest Fisheries Center. The NMFS-NWFSC series is currently used by the Northwest Fisheries Science Center.

This document should be cited as follows:

Rohan, S. K., Charriere, N. E., Riggle, B., O'Leary, C. A., and Raring, N. W. 2023. A flexible approach for processing data collected using trawl-mounted CTDs during Alaska bottom-trawl surveys. U.S. Dep. Commer., NOAA Tech. Memo. NMFS-AFSC-475, 43 p.

This document is available online at:

Document available: https://repository.library.noaa.gov

Reference in this document to trade names does not imply endorsement by the National Marine Fisheries Service, NOAA.

NOAA FISHERIES

# A Flexible Approach for Processing Data Collected Using Trawl-Mounted CTDs During Alaska Bottom-Trawl Surveys

S. K. Rohan, N. E. Charriere, B. Riggle, C. A. O'Leary, and N. W. Raring

Resource Assessment and Conservation Engineering Division
Alaska Fisheries Science Center
National Marine Fisheries Service
National Oceanic and Atmospheric Administration
7600 Sand Point Way NE
Seattle, WA 98115

**U.S. DEPARTMENT OF COMMERCE**

National Oceanic and Atmospheric Administration
National Marine Fisheries Service
Alaska Fisheries Science Center

NOAA Technical Memorandum NMFS-TM-AFSC-475

September 2023

## ABSTRACT

The Alaska Fisheries Science Center uses trawl-mounted conductivity, temperature, and depth devices (CTDs) (Sea-Bird Scientific SBE 19plus V2 SeaCAT Profiler CTD) to collect oceanographic data during bottom trawl surveys conducted aboard chartered commercial fishing vessels. Collecting CTD data in this manner minimizes sampling time and the need for specialized equipment, but it also contributes to dynamic errors in salinity profiles (e.g., salinity spikes) that are not corrected using 'typical' data processing methods. To improve dynamic error correction, we developed a data processing protocol that uses four methods to correct dynamic errors, where the best-performing method is selected for each CTD deployment based on qualitative visual inspection of processed profiles. The data processing methods include the manufacturer's recommended typical method (*Typical*), methods developed for towed and glider-borne CTDs (typical conductivity cell thermal mass correction [*Typical CTM*], temperature-salinity area [*TSA*]), and a novel method developed for this study (minimum salinity gradient [*MSG*]). We evaluated our approach by using it to process data from CTD deployments in four survey regions (eastern Bering Sea, northern Bering Sea, Aleutian Islands, Gulf of Alaska) that sampled a broad range of temperature and salinity conditions. Our results suggest that at least one data processing method corrected significant dynamic errors in at least one downcast or upcast in nearly all deployments. The best data processing method varied among profiles due to differences in temperature-salinity structure of the water column among deployments and survey regions. Based on these findings, we conclude that multiple data processing methods are needed to process trawl-mounted CTD data from Alaska bottom-trawl surveys. To facilitate data processing, we created an R package (*gapctd*) for CTD data processing that leverages functions and data structures in the widely used *oce* R package for oceanographic analysis.

## CONTENTS

# INTRODUCTION

The Alaska Fisheries Science Center's Resource Assessment and Conservation Engineering (RACE) Division's Groundfish Assessment Program (GAP) collects oceanographic data using SBE 19plus V2 CTDs (Sea-Bird Scientific, Bellevue, Washington, USA) that are attached to the bottom trawl gear during fisheries-independent bottom-trawl surveys (Cokelet 2016, Markowitz et al. 2022). Deploying CTDs in this manner has the benefit of minimizing shipboard sampling time and equipment demands compared to conventional winch-based profiling. However, the deployment method may also cause dynamic errors in sensor measurements (i.e., errors observed under changing environmental conditions) that are not adequately corrected using dynamic correction methods for winch-based profiling. Correcting these dynamic errors is necessary to ensure that trawl-mounted CTDs yield high-quality profile data that are suitable for use in research.

Dynamic error correction methods correct errors caused by stochastic sensor noise, misalignment of sensor data in space and time, thermal inertia effects, and flow reversals. Stochastic sensor noise is typically corrected using signal processing filters that reduce high frequency variation in raw data, such as low pass filters and window filters. Misalignment of sensor data occurs when individual sensors have different response rates to changes in the physical environment or sensors are physically misaligned in space. Misalignment errors can be corrected by time-shifting data from individual channels to align measurements in space and time. Thermal inertia errors occur when temperature measurements lag behind the actual temperature of a parcel of water due to heat stored in the instrument (Lueck and Pickolo 1990). These errors often lead to salinity spikes around temperature gradients because salinity calculations are based on temperature and temperature-dependent conductivity. Thermal inertia errors can be corrected using a discrete-time filter to adjust temperature or conductivity measurements to values that would be measured without latent heating effects (Morison et al. 1994). Flow reversals occur when a descending or ascending CTD slows down or reverses direction and samples a previously sampled parcel of water, often due to wave-induced ship heave. Flow reversal errors can be mitigated by omitting data collected when the profiling rate of the CTD falls below a critical threshold. The combination and order of dynamic correction methods varies depending on the instrument, deployment method, and thermohaline structure of the water column.

Dynamic correction methods developed for autonomous gliders and towed CTDs are likely to be useful for correcting dynamic errors in trawl-mounted CTD data because they also collect oblique profiles under variable profiling rates. To account for variable profiling rates in underway CTD casts,

Ullman and Hebert (2014) aligned temperature and conductivity channels by finding the time offset for temperature that maximized the correlation between the first derivative of conductivity and temperature channels with respect to time for 5-second segments of profile data. Ullman and Hebert (2014) found that the optimal alignment varied with descent rate. Ullman and Hebert (2014) also estimated parameters for a conductivity cell thermal mass correction by finding parameters that minimized the root-mean-square difference between paired salinity profiles from a UCTD and winch-based profiling CTDs. Autonomous gliders descend and ascend through the water column at an oblique angle under varying speed, which leads to variable flow rates past sensors and profiles that are separated by a distance (Garau et al. 2011). To correct for effects of variable flow rates on the unpumped thermistor and conductivity cell, Garau et al. (2011) modeled the relationship between conductivity cell thermal mass correction parameters as a function of flow speed and optimized conductivity cell thermal mass correction parameters by finding parameter values that minimized the area between temperature-salinity curves from upcast and downcast profiles. For both UCTD and glider deployments, the optimal cell thermal mass correction parameters vary among profiles. This is also the case for conventional winch deployments (Mensah et al. 2009) and Argo floats (Martini et al. 2019), where optimal corrections vary due to differences in temperature and salinity structure among profiles and different profiling rates, scan intervals, and sensor response times among instruments.

One concern with deploying CTDs on bottom-trawl survey gear is that the additional weight and drag may affect the dimensions of the trawl gear. Such changes could potentially cause biases in bottom-trawl survey catch data that are critical for fisheries stock assessments. The effects of gear modifications on fishing performance can be evaluated by comparing net measurement data that characterize the dimensions of the trawl gear between hauls with and without gear modifications (Somerton and Munro 2001).

Here, we propose an approach for processing temperature, pressure, and conductivity profile data from trawl-mounted CTDs (SBE 19plus V2) that uses four methods (*Typical*, Typical conductivity cell thermal mass correction [*Typical CTM*], Temperature-Salinity Area [*TSA*], *Minimal Salinity Gradient* [*MSG*]), with the best method selected for each profile based on visual inspection. The *Typical* method uses the typical module parameters recommended by the manufacturer[1]. The *Typical CTM* and *TSA* methods optimize module parameters using methods developed for data from autonomous gliders and towed CTDs (Garau et al. 2011, Ullman and Hebert 2014). *MSG* is a new method developed for this study

[1] Sea-Bird Scientific. (2017, July). SeasoftV2: SBE Data Processing: CTD Data Processing & Plotting Software for Windows. https://www.seabird.com/asset-get.download.jsa?code=251446. Accessed 25 February 2021.

that optimizes module parameters and, to our knowledge, has not previously been used to process CTD data. We evaluate the performance of our approach and the individual data processing methods by applying them to data collected during bottom-trawl surveys in regions that collectively include a wide range of ocean conditions (Aleutian Islands, Gulf of Alaska, eastern Bering Sea, and northern Bering Sea). Using data processing results, we examine whether the physical structure of the water column affects optimal data processing methods, as observed with other deployment methods. We also evaluate whether deploying trawl-mounted CTDs on bottom trawl gear changes the fishing performance of the trawl performance by comparing trawl geometry (net height and net width) between hauls with and without the CTD attached to the trawl. Based on our results, we evaluate whether our data processing methods adequately correct dynamic errors in trawl-mounted CTD data.

## METHODS

### Data collection

Data were collected using trawl-mounted CTDs (SBE 19plus V2 SeaCAT Profiler CTD with strain-gauge and SBE 5P/5T pump; Sea-Bird Scientific) during bottom trawl surveys conducted by NOAA's Alaska Fisheries Science Center's RACE-GAP in the eastern Bering Sea (years: 2021 and 2022), northern Bering Sea (2021 and 2022), Gulf of Alaska (2021), and Aleutian Islands (2022) (Table 1). These surveys sampled a wide range of temperature and salinity conditions that included warm and shallow brackish bays, fjords with a brackish lens, and oceanic waters along the continental slope (Fig. 1).

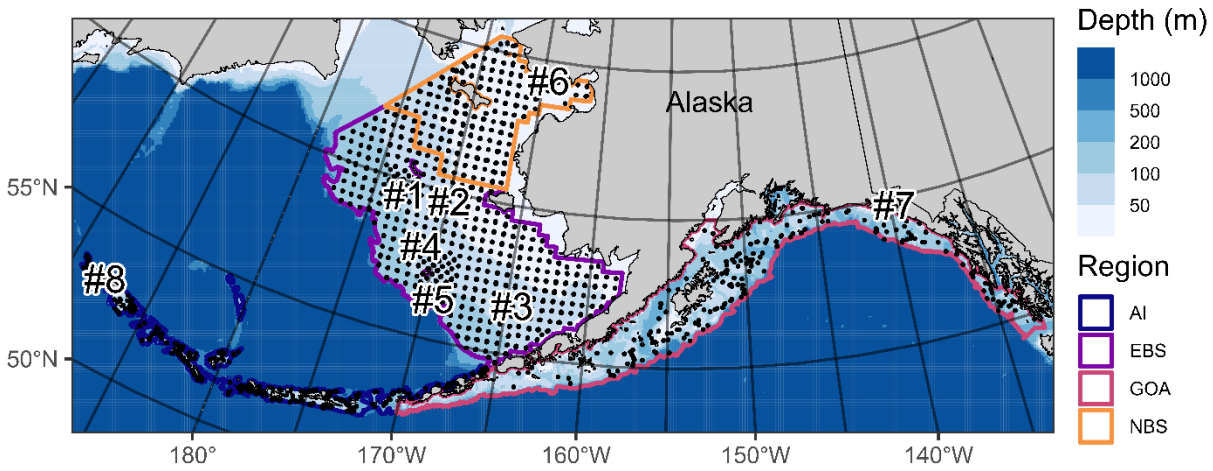


Figure 1. -- Sample and representative deployment (#1–8) locations for trawl-mounted CTD data collected during 2021 and 2022 bottom trawl surveys of the Aleutian Islands (AI), eastern Bering Sea (EBS), northern Bering Sea (NBS), and Gulf of Alaska (GOA). Dots (●) denote sample locations, outline colors denote survey regions.

To prevent damage during deployments, trawl-mounted CTDs were housed in PVC tubes that were open on both ends and with openings cut along the longitudinal axis (Fig. 2). During bottom trawl hauls, the CTD assembly (housing and CTD) was deployed inside a mesh bag affixed to the top panel of the trawl gear, approximately 0.5 to 1.0 m behind the head-rope of the trawl with the CTD plumbed for horizontal deployment and the intake port facing forward, approximately 15 cm from the anterior end of the tube. In this configuration, we expect that CTDs were oriented horizontally during deployments, but the orientation may vary with changes in trawl geometry. CTDs sampled at their maximum sampling rate (4 Hz).

Table 1. -- Number of hauls, haul depth range, and sampling dates by bottom trawl survey region.

| Region | Year | Number of deployments | Cast depth range (m) | Dates |
|---|---|---|---|---|
| Aleutian Islands | 2022 | 322 | 8–426 | Jun 9–Aug 13, 2022 |
| Eastern Bering Sea | 2021 | 380 | 18–170 | May 30–Aug 20, 2021 |
| Northern Bering Sea | 2021 | 134 | 12–76 | Jul 22–Aug 16, 2021 |
| Eastern Bering Sea | 2022 | 387 | 18–183 | May 29–Jul 29, 2022 |
| Northern Bering Sea | 2022 | 120 | 11–73 | Aug 2–Aug 20, 2022 |
| Gulf of Alaska | 2021 | 208 | 25–652 | May 30–Aug 14, 2021 |

CTD data collected during each bottom trawl haul were comprised of an oblique vertical profile during trawl deployment (downcast), a horizontal profile along the seafloor during the tow, and an oblique vertical profile during trawl retrieval (upcast). The proximity of the CTDs to the seafloor during deployments varied among surveys due to differences in trawl gear designs. The eastern Bering Sea shelf and northern Bering Sea surveys used an 83-112 eastern otter trawl with a 1.8 to 2.5 m headrope height while the net was on-bottom in fishing configuration. The Gulf of Alaska and Aleutian Islands surveys used a Poly Nor'Eastern trawl with a fishing height of 5.5 to 7.5 m while the trawl was in fishing configuration. All surveys towed at a target speed of 3.0 knots while fishing (acceptable range of 2.8 to 3.2 knots). The eastern Bering Sea shelf and northern Bering Sea surveys towed for 30 minutes per haul while the Gulf of Alaska and Aleutian Islands surveys towed for 15 minutes. Consequently, downcasts and upcasts were typically ~2.8 km apart in the eastern Bering Sea and northern Bering Sea and ~1.4 km apart in the Gulf of Alaska and Aleutian Islands.

An acoustic net mensuration system (Marport Deep Sea Technologies Inc.) was used to measure net spread and height (in meters) during trawl survey operations (von Szalay and Raring 2020, Markowitz et al. 2022). Net spread data were measured by port and starboard spread sensors attached forward of the dandyline and upper breastline junctions, while net height was measured from the headrope to the seafloor with a single height sensor. Mean net spread was calculated from raw measurements using protocols described by Lauth and Kotwicki (2014).

Figure 2. -- SBE 19plus V2 SeaCAT Profiler CTD in a PVC housing attached behind the trawl headrope during the 2022 eastern Bering Sea survey.

## CTD Data Processing

Our aim was to develop a consistent, reproducible, and effective method for correcting dynamic errors in vertical profiles of temperature, salinity, and pressure in trawl-mounted CTD data. Dynamic errors include stochastic noise in raw data, erroneous salinity spikes around strong temperature gradients, unrealistic density inversions, and misalignment of temperature and salinity profiles. Although we initially attempted to correct dynamic errors with data processing modules in SBE Data Processing software using typical parameters recommended by the manufacturer (Table 2), the approach often did not correct dynamic errors in profiles. We also attempted to develop a suite of dynamic correction methods with varying parameters for modules since optimal parameters can vary depending on temperature and salinity conditions (e.g., Mensah et al. 2009). However, this approach

was not suitable for addressing the wide range of environmental and operating conditions across the survey regions and survey vessels.

Table 2. --Typical Sea-Bird Data Processing software module parameter values that are recommended by the manufacturer for processing data from a pumped SBE 19plus V2 SeaCAT Profiler CTD*.

| **Module parameter** | **Typical value** | **Typical range** |
|---|---|---|
| *Low pass filter module* | | |
| Time constant, Temperature | 0.5 | |
| Time constant, Conductivity | 0.5 | |
| Time constant, Pressure | 1.0 | |
| *Align module* | | |
| Temperature alignment, $t_T$ | -0.5 | 0.0 – -1.0 |
| Conductivity alignment, $t_C$ | 0.0 | 0.0 – -0.1 |
| *Conductivity cell thermal mass correction module* | | |
| Initial conductivity error, $\alpha$ | 0.04 | |
| Time decay constant, $\beta$ | 1/8 | |

* Sea-Bird Scientific. (2017, July). SeasoftV2: SBE Data Processing: CTD Data Processing & Plotting Software for Windows. https://www.seabird.com/asset-get.download.jsa?code=251446. Accessed 25 February 2021.

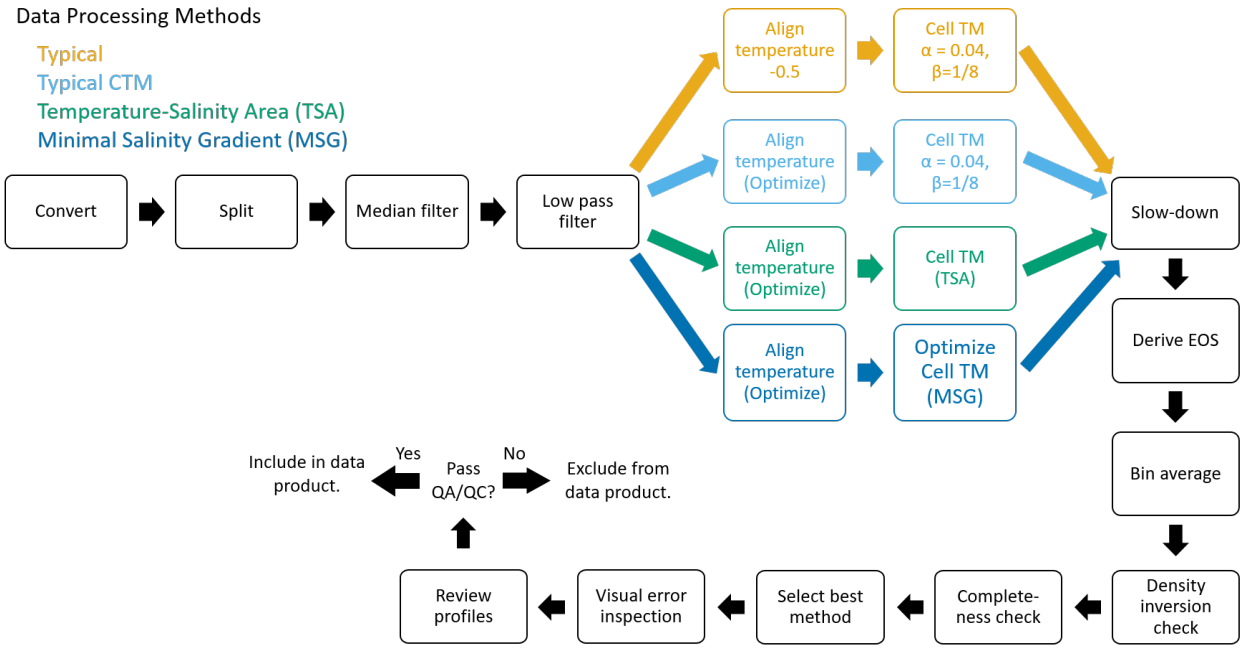


Figure 3. -- Data processing method workflows for CTD data.

To process the CTD data, we developed a data processing method that combines dynamic correction modules from SBE Data Processing software and dynamic correction optimization methods based on those developed for processing data from UCTDs and glider-borne CTDs. Data processing modules are applied sequentially using the workflow shown in Figure 3. Data processing steps are described in subsections 2.2.1–2.2.16. Data were processed using the *gapctd* R package version 1.3.4, which was developed for this study. The package and example code for data processing are available at http://www.github.com/afsc-gap-products/gapctd.

## Convert raw CTD data

Raw data files are converted to retrieve temperature (°C), conductivity (S $m^{-1}$), pressure (dbar), and time elapsed (seconds) channels.

## Split

Casts are split into downcast, bottom, and upcast sections based on time elapsed and haul event times that are recorded at-sea. Downcasts include data collected between the beginning of trawl operations and on-bottom time plus 30 seconds. Upcasts include data collected between the beginning of haul back minus 30 seconds and the end of trawl operations. These time buffers accommodate changes in geometric configuration while the net is reaching or leaving the bottom. The bottom data includes data collected between the end of the downcast and beginning of the upcast. Scans with pressure < 0.5 dbar are removed from downcast and upcasts.

## Median window filter

Median window filters remove outliers in noisy data by replacing individual scan measurements with the median value within a time window around a scan. Using a larger time window tends to over-smooth actual variation while a smaller window may fail to remove outliers. We use a five scan (1.25 s) window for median filtering conductivity, temperature, and pressure channels because we determined through trial and error that the window removes transient spikes without evident over-smoothing. At typical descent and ascent speeds for our sampling method, the five-scan window corresponds with ~0.20–0.66 m of vertical travel or a vertical velocity of ~0.16 to 0.53 $m \cdot s^{-1}$.

## Low pass filter

Low pass filters are useful for reducing high-frequency noise in scan data. The functional form of the low pass filter is

$$y(n) = A\big(x(n) + x(n-1)\big) - By(n-1) \tag{1}$$

$$B = A\left(1 - \frac{2\omega}{f_s}\right) \tag{2}$$

$$A = \left(1 + \frac{2\omega}{f_s}\right)^{-1} , \tag{3}$$

where $y(n)$ is the output for the current step, $y(n-1)$ is the output from the previous step, $x(n)$ is the input from the current scan, $x(n-1)$, is the input from the previous scan, $\omega$ is a time constant, and $f_s$ is the sampling interval in seconds (i.e., 0.25 s at 4 Hz). We low pass filter temperature, conductivity, and pressure channels with time constants of 0.5 s, 0.5 s, and 1.0 s, respectively, following the manufacturer's recommended settings. We run the low pass filter forward then backwards through the data to prevent time-shifting the data.

### Align

The *Align* module uses the alignment method from SBE Data Processing software to time-shift measurements relative to pressure. Misalignment of temperature, salinity, and pressure data causes errors in salinity, such as salinity spikes and unrealistic density inversion. Misaligment occurs when sensors are physically misaligned in space or response times differ among sensors. Time-shifting data can align measurements and mitigate these errors. The SBE 19plus V2 temperature sensor responds slower than the conductivity and pressure sensors so the manufacturer recommends advancing the temperature channel by 0.0–1.0 s (typically 0.5 s) to correct the alignment, depending on operating conditions.

### Optimize temperature alignment

Temperature and salinity tend to change synchronously at density gradients (Barth et al. 1996, Ullman and Hebert 2014). In the *Typical CTM*, *TSA*, and *MSG* methods, optimal temperature alignment offsets are estimated by finding the offset that maximizes the correlation between the first derivatives of temperature ($dT/dt$) and conductivity ($dC/dt$). This approach is similar to Barth et al. (1996), Ullman and Hebert (2014), and Dever et al. (2020) but is applied to full profiles instead of windows of scans within profiles (we evaluate scan window approaches in the Effect of profiling rates on temperature alignment section). Temperature offsets are optimized for each upcast and downcast by finding the offset between -1.00 to +1.00 s that maximizes the Pearson product moment correlation ($r^2$) between $dT/dt$ and $dC/dt$ to 0.01 s precision.

## Conductivity cell thermal mass discrete time filter

The conductivity sensor on the SBE19plus V2 has higher thermal inertia than the temperature sensor, which can cause a lag in temperature-dependent conductivity measurements as the CTD passes through temperature gradients. These errors often result in 'spikes' in salinity profiles that are in opposite directions (positive and negative) between downcasts and upcasts. These errors can be corrected using a discrete-time filter to adjust measurements to match conductivity that would be measured at the true water temperature outside of the conductivity cell, $\widehat{C(n)}$, as:

$$\widehat{C(n)} = C(n) + C_T(n)\,, \tag{4}$$

where $C(n)$ is the measured conductivity and $C_T(n)$ is the discrete-time filter conductivity correction for scan $n$ (Lueck 1990). Following the manufacturer's correction procedures, discrete-time filter conductivity corrections are calculated as:

$$C_T(n) = -bC_T(n-1) + \frac{a\left[1 + 0.006[T(n) - 20][T(n) - T(n-1)]\right]}{10} \tag{5}$$

$$b = 1 - 2a\alpha^{-1} \tag{6}$$

$$a = 2\alpha[f_s\beta + 2]^{-1}\,, \tag{7}$$

where $T(n)$ is measured temperature, $f_s$ is the CTD sampling interval (i.e., 0.25 s), $\alpha$ is the initial conductivity error, and $\beta$ is a time decay constant. The manufacturer suggests that typical parameters for conductivity cell thermal mass corrections for the SBE 19plus V2 are $\alpha = 0.4$ and $\beta^{-1} = 8$.

## Optimize conductivity cell thermal mass parameters

When 'typical' values of conductivity cell thermal mass correction parameters (*a* and *b*) do not adequately correct dynamic errors in salinity profiles, different parameter values can be useful for mitigating dynamic errors (Mensah et al. 2009). Therefore, we used two methods (*Temperature-Salinity Area* and *Minimal Salinity Gradient*) to estimate optimal conductivity cell thermal mass correction parameters to improve salinity profiles in cases where typical values did not adequately correct dynamic

errors. The *Temperature-Salinity Area* method optimized parameters by finding values of $\alpha$ and $\beta$ that minimized the area between temperature-salinity curves from downcasts and upcasts (Garau et al. 2011).

Profiles with erroneous salinity spikes have unreasonably large derivatives in salinity with respect to pressure. Salinity spikes can be corrected using optimized $\alpha$ and $\beta$ parameters for conductivity cell thermal mass correction, which also reduces derivatives in salinity with respect to pressure. Here, we introduce the *Minimal Salinity Gradient* method, where $\alpha$ and $\beta$ parameters are optimized by minimizing the absolute sum of the rate of change in salinity with pressure (i.e., derivative in salinity with respect to pressure), which we define as:

$$Minimum\ Salinity\ Gradient = \sum_{i=2}^{N_B} \left| \frac{S_i - S_{i-1}}{P_i - P_{i-1}} \right| , \quad (8)$$

where $N_B$ is the number of pressure bins in a cast, $P_i$ is pressure (dbar) in bin $i$, and $S_i$ is average salinity in bin $i$. Figure 4 shows a conceptual illustration of how the area between temperature-salinity curves and minimum salinity gradient are calculated using hypothetical temperature and salinity profiles.

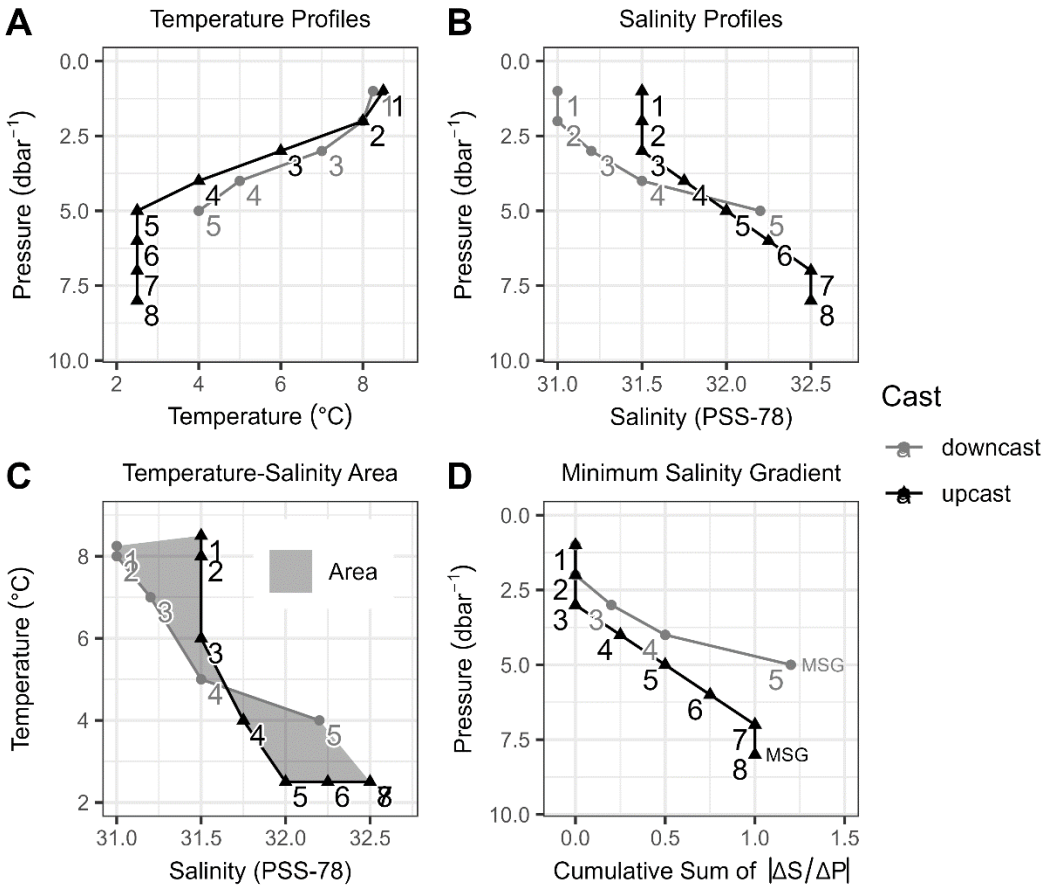


Figure 4. -- Conceptual example of Temperature-Salinity Area and Minimum Salinity Gradient method calculations. Panels show: (A) hypothetical temperature profiles, (B) hypothetical salinity profiles, (C) temperature-salinity plot with shading showing the area between downcast and upcast curves, (D) minimum salinity gradient; that is, the cumulative sum of rates of change in salinity with respect to pressure for an entire profile where 'MSG' denotes the total for a profile. On each panel, numbered shapes denote the pressure (dbar-1) for a value within a downcast (grey circles) or upcast (black triangles).

For both methods, we estimated optimal parameters using the Broyden-Fletcher-Goldfarb-Shanno (BFGS) optimization algorithm with box constraints (Byrd et al. 1995). Due to issues with local minima in parameter searches for some profiles, we found initial parameter starting values for each deployment (*T-S Area* method) or profile (*MSG* method) using a grid search across all combinations of $\alpha$: $\{0.001, 0.01, 0.02, \mathbf{0.04}, 0.08, 0.12\}$ and $\beta^{-1}$: $\{1, 2, 4, \mathbf{8}, 12, 24\}$ with the manufacturer's suggested typical values in bold type. The optimal set of parameters for the optimization was then used for the BFGS optimization. The box constraints for optimization were $0 \leq \alpha \leq 1$ and $0.1 \leq \beta^{-1} \leq 45$. The

upper 4 m of the water column were excluded from optimization because large errors and small-scale variability near the surface exerted undue influence on parameter estimates.

### Slowdown

Slowdowns or reversals of the CTD during downcasts or upcasts can cause turbulent mixing and flow reversals around the CTD that produce errors in temperature and salinity data. These slowdowns and reversals result from wave motion or changes in trawl winch speeds. Excluding data collected during slowdowns and reversals can mitigate dynamic errors. Slowdowns and reversals can be detected when ascent or descent speeds fall below a critical threshold. Similar to the *Loop edit* module in SBE Data Processing software, the *Slowdown* module flags scans where the mean profiling speed for a scan, based on a window around a scan, falls below a user-specified threshold.

The manufacturer recommends that the optimal profiling speed for the SBE 19 plus V2 is 0.5 to 2.0 m $s^{-1}$ but that slower speeds (0.1 to 0.2 m $s^{-2}$) can be suitable in calm seas. The mean profiling speed for our trawl-mounted CTD data was 0.33 m $s^{-1}$, with 95% of profiles sampled between 0.18 and 0.49 m $s^{-1}$. However, there was depth-dependent variation in profiling speeds and the slowest speeds generally occurred at the surface and bottom. Preliminary analysis suggested that slowdowns near the surface with its larger temperature and salinity gradients had a large impact on temperature and salinity, whereas slowdowns near the bottom (while the net was settling into fishing configuration) typically had a low impact. Based on preliminary analysis, we flag scans that are not in the bottom 3-m of a profile where the mean speed for a five-scan (1.25 s) window is below 0.1 m $s^{-1}$.

### Derive

Practical salinity, density, potential density, absolute salinity, sound speed, and squared buoyancy frequency are derived from temperature, conductivity, and pressure using functions in the *oce* R package (Kelley and Richards 2022, Kelley et al. 2022).

### Bin average

Averages for all variables are calculated for 1-m depth bins but with data flagged by the *Slowdown* module and from the shallowest 0.5 m omitted.

## Density inversion check

Density inversion errors occur in some CTD profiles, likely due to shed wake and turbulence. Density inversion errors were automatically assigned when $N^2$ < -1 × $10^{-5}$ radians$^2$ s$^{-2}$ at depths > 20 m. Density inversion errors are corrected by automatically detecting, removing, and linearly interpolating errors then recalculating derived quantities ($S$, $N^2$, $\rho$, $\rho_\theta$). Interpolated data are flagged as corrected by the density inversion check. At depths < 20 m, bins with $N^2$ < -1 × $10^{-5}$ radians$^2$ s$^{-2}$ are flagged as potential errors for quality assurance purposes but are not removed.

## Completeness check

Profiles do not contain data from the full water column if the CTD shuts down during a deployment or data from numerous depth bins are flagged by the *Slowdown* module. To avoid including incomplete profiles in data products, cast data are excluded if there are no data for > 12.5% of depth bins sampled during a cast or if > 10% of profile data are flagged, even if flags denote corrected errors.

## Select best method

Profiles from the four processing methods (*Typical*, *Typical CTM*, *T-S Area, MSG*) are visually inspected and the method that produces the profile with the fewest obvious dynamic errors is selected for subsequent manual error correction. If the more than one method produces nearly identical 'best' profiles, selection is prioritized in the following order: *Typical* (highest priority), *Typical CTM*, *TS Area, MSG* (lowest priority).

## Visual error inspection

Downcast and upcast profile data processed using the best method for each deployment are visually inspected for remaining dynamic errors in density and salinity. Errors that span 1–2 consecutive depth bins are manually identified and removed, then conductivity and temperature are interpolated using linear interpolation. Derived quantities ($S$, $N^2$, $\rho$, $\rho_\theta$) are then re-calculated using the derive module.

## Review profiles

We select downcasts and upcasts to include in the data product based visual inspection of temperature, salinity, and density profiles from each deployment. For each deployment, the downcast, upcast, both casts, or no casts are selected depending on the prevalence of dynamic errors and unrealistic density inversions in the profiles.

## Effect of profiling rates on temperature alignment

When profiling rates (dbar $s^{-1}$ or m $s^{-1}$) vary within a cast, an alternative to using a single temperature alignment parameter for an entire profile can be to vary the alignment parameter within segments (i.e., scan windows) of a cast based on the profiling rate within each segment (Ullman and Hebert 2014). Therefore, we evaluated whether the optimal temperature alignment parameter varied within casts as a function of profiling speed by estimating optimal alignment parameters for segments of individual casts. To do so, we estimated temperature alignment parameters for segments of 16, 24, 40, and 60 scans (4–15 s). For each scan range, we fit a generalized additive model between a cubic regression spline of profiling speed (predictor) and the optimized temperature alignment for all segments of all casts. We considered that a strong relationship between profiling speed and optimal temperature alignment parameters would indicate that we should consider data processing methods that used profiling speed as a basis to estimate temperature alignment.

## Evaluating performance in representative deployments

We evaluated the performance of our approach to data processing by comparing results among profiles processed using each of the four methods. For the sake of brevity, we focus on processing results from eight deployments that represent the range of sampling conditions observed in our study area (Table 3) rather than presenting results from all 1,551 deployments. The profiles include a shallow brackish bay (Norton Sound), a glacial bay with a low salinity lens (Yakutat Bay), an open-ocean station at the western end of the Aleutian Islands archipelago, and five 2-3 layer stratified water columns with different rates of change in temperature and salinity around the pycnocline (eastern Bering Sea). The EBS is over-represented compared to other regions because the sharp density gradients in the region tended to produce erroneous salinity spikes at a higher rate than in other regions.

Table 3. --Representative deployments showing the deployment number, survey region, sampling date, latitude in decimal degrees north, and longitude in decimal degrees east, maximum temperature, T (°C), and salinity, S (PSS-78), range (maximum minus minimum) among casts, and maximum temperature gradients and salinity gradients among casts. Deployment locations are shown in Figure 2.

| | | | Coordinates | | Max. range | | Max. gradient | |
|---|---|---|---|---|---|---|---|---|
| # | Region | Date | Lat. | Lon. | T (°C) | S ($m^{-1}$) | T (°C $m^{-1}$) | S ($m^{-1}$) |
| 1 | EBS | Jul 8, 2021 | 59.51 | -172.90 | 6.32 | 0.14 | 1.530 | 0.005 |
| 2 | EBS | Jul 4, 2022 | 59.68 | -169.93 | 5.55 | 0.03 | 1.154 | 0.001 |
| 3 | EBS | Aug 19, 2021 | 56.66 | -164.60 | 8.51 | 0.20 | 1.239 | 0.019 |
| 4 | EBS | Jul 6, 2022 | 57.99 | -170.97 | 6.85 | 0.30 | 0.657 | 0.012 |
| 5 | EBS | Jul 8, 2022 | 56.37 | -169.45 | 4.09 | 0.73 | 0.202 | 0.013 |
| 6 | NBS | Aug 6, 2021 | 64.33 | -164.57 | 4.73 | 5.36 | 0.986 | 0.053 |
| 7 | GOA | Jul 16, 2021 | 59.76 | -139.69 | 5.85 | 9.89 | 0.800 | 0.181 |
| 8 | AI | Jul 30, 2022 | 52.95 | 172.17 | 7.67 | 1.25 | 0.327 | 0.011 |

## Effect of trawl-mounted CTD on trawl height

We hypothesized that the CTD on the trawl would affect the height of the trawl in fishing configuration due to the additional weight and drag caused by the CTD and housing. We evaluated support for this hypothesis using a Bayesian linear mixed effects model to estimate the effect of the CTD on trawl height using data from 278 hauls from a single vessel during the 2021 Gulf of Alaska survey. In our model,

$$\boldsymbol{H_i} = K\boldsymbol{X_i} + \boldsymbol{k_i}\boldsymbol{Z_i} + \varepsilon_i$$
$$\varepsilon \sim N(0, \sigma^2)$$
$$\boldsymbol{k_i} \sim N(0, D_i) \ ,$$

where $\boldsymbol{H_i}$ is the average trawl height while the net was on bottom for deployment $i$, $K$ is a fixed effect of the CTD on trawl height, $\boldsymbol{X_i}$ is a binary design matrix of treatment effects indicating whether or not a CTD was deployed on the trawl, $\boldsymbol{k_i}$ is a random effect of average fishing height for an individual trawl net, and $\boldsymbol{Z_i}$ is a binary design matrix indicating the net number. Random effects were necessary for each net because fishing heights differ among nets due to subtle differences in construction or wear. We

used weakly informative prior distributions for fixed and random effects parameters and estimated model parameters using Metropolis-Hasting Markov Chain Monte Carlo with four 2,000 sample chains (1,000 burn-in samples, 1,000 real samples) using the R package *rstanarm* (Goodrich et al. 2022).

## RESULTS

### Overall

Profiles processed using the *Typical* method were selected as the 'best' more often (80.9%) than profiles processed with the *Typical conductivity cell thermal mass correction* (*Typical CTM*; 6.6%), *Temperature-Salinity Area* (*TSA*; 8.2%), or *Minimal Salinity Gradient* (*MSG*; 4.4%) methods (Table 4). The *Typical* method was selected at a higher rate in the Gulf of Alaska (99.0%) and Aleutian Islands (99.1%) than in the eastern Bering Sea and northern Bering Sea (69.8% in 2021; 73.0% in 2022). Differences in selection rates among methods do not accurately reflect performance differences among methods because profiles from multiple methods were often extremely similar because optimized parameters were often close or identical to profiles processed using the *Typical* method and the *Typical* method was selected if it had similar performance to other the 'best' methods. All methods tended to produce extremely similar profiles when the water column was fully mixed or weakly stratified. Downcasts (81.0%; 1,256 out of 1,551) were selected at a higher rate than upcasts (44.9%; 696 out of 1,551) and both casts were selected in only 25.9% of deployments.

Table 4. -- Best data processing method among deployments, by region and year.

| | | **Best processing method** | | | |
|---|---|---|---|---|---|
| **Region** | **Year** | **Typical** | **Typical CTM** | **TSA** | **MSG** |
| AI | 2022 | 99.1% | 0.0% | 0.6% | 0.3% |
| EBS+NBS | 2021 | 69.8% | 10.7% | 12.8% | 6.6% |
| EBS+NBS | 2022 | 73.0% | 9.3% | 11.6% | 6.1% |
| GOA | 2021 | 99.0% | 0.0% | 0.0% | 1.0% |
| All | All | 80.9% | 6.6% | 8.2% | 4.4% |

The proportional differences in best data processing methods among regions (Table 4) were primarily a result of regional differences in the rates of change in temperature in profiles (Fig. 5A-B). The average maximum rate of change in temperature was lower among *Typical* method profiles (0.42 °C $m^{-1}$; 0.12 °C $s^{-1}$) that were selected as the best than *Typical CTM* (0.74 °C $m^{-1}$; 0.22 °C $s^{-1}$), *TSA* (0.84 °C $m^{-1}$; 0.24 °C $s^{-1}$), or *MSG* (0.76 °C $m^{-1}$; 0.21 °C $s^{-1}$) methods (Fig. 5C-D). Consequently, the eastern Bering Sea and northern Bering Sea had the lowest rates of the *Typical* method being selected as best because these regions had higher average maximum rates of change in temperature (0.62 °C $m^{-1}$) than the Gulf of Alaska (0.30 °C $m^{-1}$) or Aleutian Islands (0.15 °C $m^{-1}$).

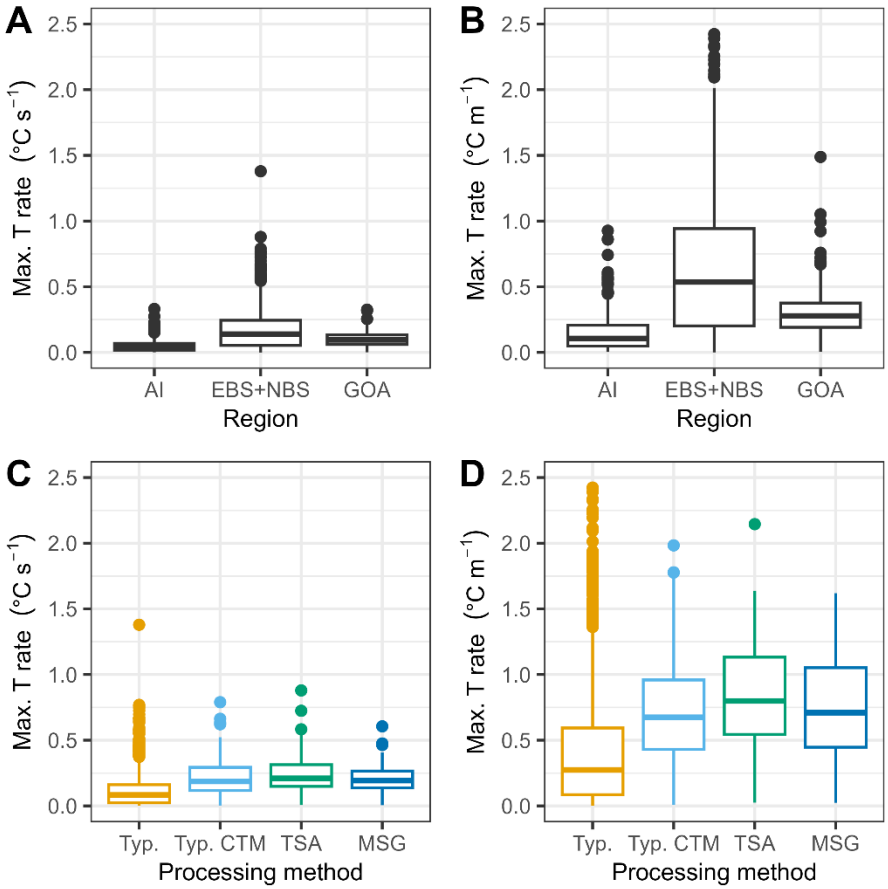


Figure 5. -- Boxplots of maximum rates of change in temperature among 'best' profiles by survey region (panels A-B) and data processing method (panels C-D). Data processing methods are *Typical* (Typ.), *Typical CTM* (Typ. CTM), *Temperature-Salinity Area* (TSA), and *Minimal Salinity Gradient* (MSG). Tukey-style boxplots show the median (center horizontal line), quartiles 1 and 3 (horizontal box end lines) , range of values within 1.5 times the interquartile range of quartiles 1 and 3 (vertical lines), and outliers exceeding 1.5 times the interquartile range (points).

Estimated temperature alignment and conductivity cell thermal mass correction parameters varied among profiles where module parameters were estimated (i.e., *Typical CTM*, *TSA*, *MSG*; Fig. 6). The optimal temperature alignment parameter had a mode within 0.1 s of the typical value recommended by the manufacturer (-0.5 s; i.e., two scan interval at 4 Hz) and a secondary peak at approximately -1.0 s (four scan intervals) for *Typical CTM*, *TSA*, and *MSG* methods. The *TSA* method had a mode in the initial conductivity error parameter ($\alpha$) at 0.01, while the *MSG* had a mode at 0.1, which suggests *TSA* performed better when the magnitude of initial conductivity error was smaller than assumed in the *Typical* method. *MSG* performed better when errors were larger than the *Typical* method value. Both methods also had modes at $\alpha = 0.001$. Modes in the time decay constant ($\beta$) occurred at 1/2, 1/24, and 1/45 for *TSA* and 1/2, 1/8, and 1/24 for *MSG*. For both *TSA* and *MSG* methods, high densities of values in the initial conductivity error ($\alpha$) and inverse of time decay constant ($\beta^{-1}$) parameters that were lower than the manufacturer's suggested values suggests, on average, conductivity errors were smaller and did not persist for as long as assumed by the manufacturer's typical parameterization. Meanwhile, the occurrence of larger values of $\alpha$ and $\beta^{-1}$ suggest that some errors were larger and persisted longer than assumed by the typical parameterization. However, effects of $\alpha$ and $\beta$ cannot be fully interpreted independently from each other because a decrease in one can be offset by an increase in the other (e.g., Martini et al. 2019).

Profiling speeds varied with depth and were generally slowest near the surface and bottom (Fig. 7). Upcast profile speeds were faster than downcasts by 0.005 to 0.041 m $s^{-1}$, depending on the vessel. Mean profiling speeds varied among vessels (0.30–0.45 m $s^{-1}$) due to differences in station depths among survey regions and differences in trawl winch power and different procedures used to deploy and retrieve the bottom trawl gear. In the GOA, EBS, and NBS, profiling speeds typically slowed down at 10 to 20 m depth, which corresponds with depths where trawl winch speeds are changed during deployment and retrieval.

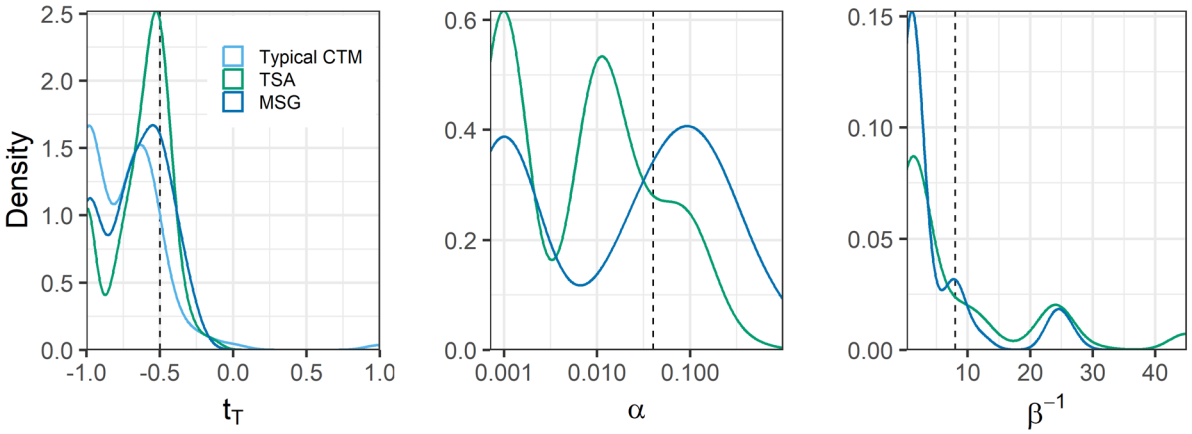


Figure 6. -- Density distribution of optimized temperature alignment ($t_T$) and conductivity cell thermal mass correction ($\alpha$ and $\beta$) parameters among selected 'best' casts that used optimization methods (i.e., *Typical CTM*, *TSA*, *MSG*). Dashed vertical lines denote typical values recommended by the manufacturer.

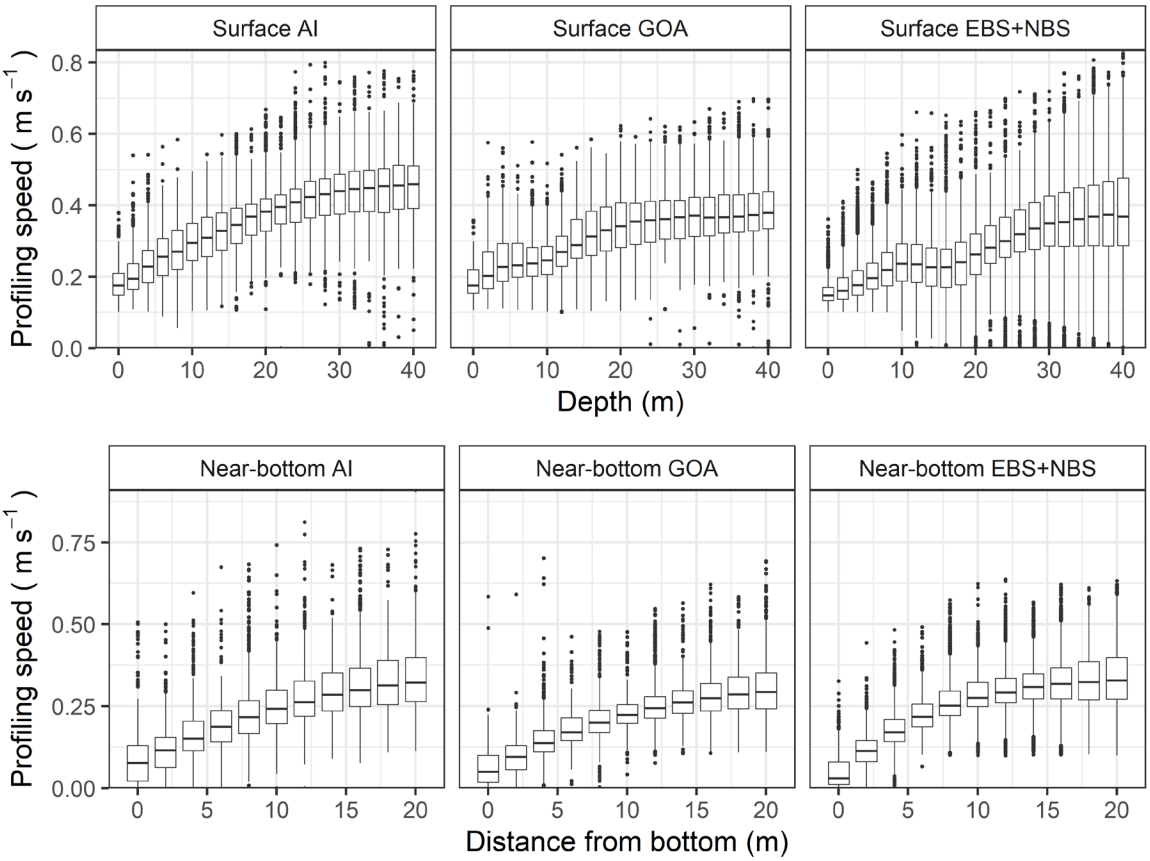


Figure 7. -- Boxplots of CTD profiling speeds (m s$^{-1}$) near the surface (depth < 40 m) and near-bottom (within 20 m of the fishing depth of the trawl), by survey region. Profiling speed observations binned by 2-m depth increments. Tukey-style boxplots show the median (center horizontal line), quartiles 1 and 3 (horizontal box end lines), range of values within 1.5 times the interquartile range of quartiles 1 and 3 (vertical lines), and outliers exceeding 1.5 times the interquartile range (points).

## Effect of profiling rate on temperature alignment

Profiling rate did not have a clear effect on temperature alignment based on generalized additive models between profiling rate and estimated temperature offset, explaining only 1.1–1.3% of the deviance in temperature offset (Fig. 8). For windows of 16, 24, 40, or 60 scans, optimized temperature offsets were usually between -0.51 and -0.55 s for profiling rates between 0.1 dbar $s^{-1}$ and 1.5 dbar $s^{-1}$.

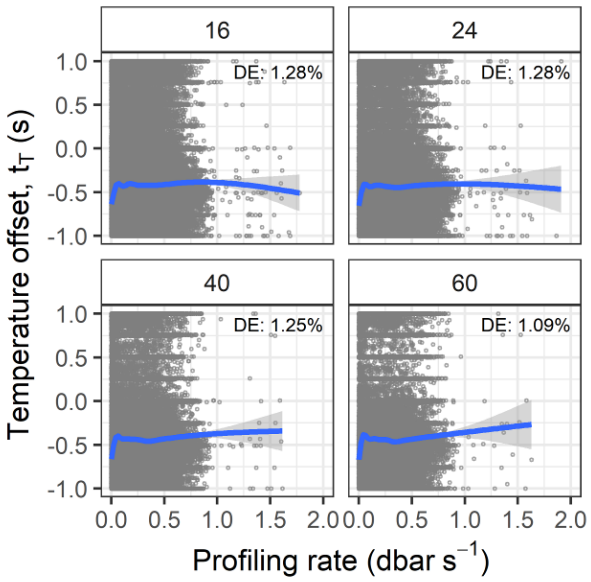


Figure 8. -- Profiling rate (dbar $s^{-1}$) versus estimated temperature alignment offsets, $t_T$, (s) for segments of 16, 24, 48, and 60 scans. Panels show estimates for individual segments (points), generalized additive model fitted mean (blue line), +/- 1 standard error (shading), and percent deviance explained (DE; top right of each panel).

## Performance in representative deployments

Deployment #1 profiled a water column with stair-casing temperature and salinity that had a surface mixed layer extending to 14 m and steps in temperature and salinity at 28 m and 44 m (Fig. 9A, 9B). Prior to temperature alignment, erroneous salinity spikes occurred at the same depths as temperature and salinity steps. All data processing methods produced a considerable reduction in salinity spikes after temperature alignment and conductivity cell thermal mass correction. However, *Typical*, *Typical CTM*, and *TSA* methods appeared to overshoot salinity at the thermocline and small

salinity spikes remained in *Typical* method downcast and upcast profiles and *Typical CTM* method upcasts. The *MSG* method yielded profiles without salinity spikes or unrealistic density inversions (Fig. 9C) so we selected the *MSG* downcast and upcast profiles as the best casts.

Figure 10 shows the results of conductivity cell thermal mass corrections applied to two casts from Deployment #1 to illustrate the effect of *Typical CTM*, *TSA*, and *MSG* methods. After optimizing temperature alignment (beginning of conductivity cell thermal mass correction), downcast salinities were generally higher than upcast salinities, the area between temperature-salinity curves was 0.16 (Fig. 10A), and the minimal salinity gradients were 0.2445 and 0.2906 for downcasts and upcasts, respectively (Fig. 10D). After alignment, the downcast salinity appeared to overshoot the presumably correct salinity from 45 to 60 m depths. Using the *Typical CTM* method increased the area between temperature-salinity curves to 0.18 (Fig. 10B), increased minimal salinity gradient for the upcast to 0.4388, and decreased minimal salinity gradient to 0.2322 (Fig. 10E). The *Typical CTM* method reduced but did not entirely remove the downcast salinity spike at 14 m and corrected the salinity overshoot from 45 to 60 m (Fig. 10D–E). In the upcast, the increases in temperature-salinity area and upcast minimal salinity gradient caused by the *Typical CTM* method were associated with increasing salinity spikes. The *Typical CTM* method shifted downcast and upcast salinity curves closer together and the downcast had lower salinity than the upcast for portions of the profiles. Optimizing conductivity cell thermal mass correction using the *TSA* method decreased the total area between temperature-salinity curves from 0.16 to 0.07 and shifted downcast and upcast salinity profiles closer together (Fig. 10C), but did not correct salinity spikes (as described above; Fig. 9B). The *MSG* method decreased the downcast minimal salinity gradient from 0.2445 to 0.2035 and the upcast from 0.2906 to 0.2898 (Fig. 10F). The *MSG* method reduced salinity spikes in the downcast compared to the spikes after temperature alignment, although a spike remained at 14 m (Fig. 10D). Overall, the *Typical CTM* method was the most effective method for correcting the salinity overshoot in the downcast from 45 to 60 m (Fig. 10E) and the *MSG* method was most effective for correcting salinity spikes (Fig. 10F).

Deployments #2 and #3 profiled two-layer stratified water columns with a steep thermocline gradient (Figs. 11A, 12A) and resulted in erroneous salinity spikes around the thermocline (Figs. 11B, 12B). Salinity spikes of 0.1–0.2 (Deployment #2) and 0.7 (Deployment #3) remained after median and low-pass filtering, but aligning temperature reduced salinity spikes to < 0.1 in all methods. Subsequent conductivity cell thermal mass correction increased salinity spikes in the *Typical*, *Typical CTM*, and *MSG* methods, but not the *TSA* downcast in Deployment #2 or the *TSA* downcast and upcast in Deployment #3. The *MSG* method over-smoothed Deployment #3 downcast salinity, resulting in a more gradual

change in salinity than observed with other methods. After slowdown corrections and automated QA/QC checks, salinity spikes remained in all Deployment #2 casts except the *TSA* downcast, but spikes were mitigated *Typical CTM* and TSA methods for deployment #3. Over-smoothed Deployment #3 downcast salinity in *MSG* remained after the slowdown corrections. There were no problematic density inversions in final profiles from any of the methods (Figs. 11C, 12C). Based on visual inspection of salinity and density curves, the best casts were the TSA downcast in Deployment #2 and both *Typical CTM* casts in Deployment #3.

Deployment #4 provides an example of small-scale differences in thermohaline structure between downcasts and upcasts, as the bottom layer temperature was ~0.7°C during the downcast and ~1.7°C during the upcast (Fig. 13A). Changes in salinity occurred at different depths between casts (10–15 m deeper in the upcast; Fig. 13B) although the thermocline occurred at same depth. Aligning temperature reduced variability in salinity below the thermocline across all methods and all methods yielded similar profiles. None of the methods resulted in density inversions (Fig. 13C). The *Typical* downcasts and upcasts were selected as the best casts because all data processing methods had similar results.

Deployment #5 sampled a three-layer stratified water column in the EBS with gradual temperature changes in the upper water column (Fig. 14A). Temperature and salinity (Fig. 14B) profiles were similar between downcasts and upcasts, with profiles from both casts crossing each other multiple times. All methods that optimized temperature alignment or conductivity cell thermal mass correction parameters (*Typical CTM*, *TSA*, *MSG*) appeared to over-correct salinity and cause small density inversions in upcasts (Fig. 14C), whereas the *Typical* method yielded smooth downcast and upcast profiles. Therefore, *Typical* the downcast and upcast were selected as the best casts.

Deployment #6 collected profiles in Norton Sound, a shallow inlet in the northern Bering Sea with low salinity surface waters caused by the inflow of numerous rivers, including the large Yukon River (Kearney, 2019). Downcast and upcast profiles had large changes in both temperature (Fig. 15A) and salinity (Fig. 15B), with 12.8–13.3 °C near-surface temperatures, 8.6°C bottom temperature, 22.4–22.8 near-surface salinity, and 27.6–28.5 bottom salinity. Differences in temperature and salinity profiles between the downcast and upcast show that the profiles were obtained from water with different properties, which is not unusual given the large horizontal temperature and salinity gradients in Norton Sound, but suggests homogeneity assumptions of the *TSA* method were violated. Despite these large changes in temperature and salinity, all data processing methods yielded similar profiles with no

evidence of dynamic errors in salinity (Fig. 15B) or density inversions (Fig. 15C). As such, upcasts and downcasts processed using the *Typical* method were selected as the best casts.

Deployment #7 profiled a two-layer stratified water column with a steep surface temperature gradient and gradual deep temperature gradient (Fig. 16A) in Yakutat Bay, a glacial fjord system in the Gulf of Alaska with a freshwater lens (Fig. 16B; Arimitsu et al. 2016). Between 10 and 20 m, there was a 2°C difference between downcast and upcast profiles. There was a large salinity difference between the surface (21.8) and the bottom (31.7). Similar to Norton Sound, Yakutat Bay is characterized by strong horizontal gradients in temperature and salinity, such that assumptions of the *TSA* method are likely violated. All methods yielded similar temperature and salinity profiles with negligible differences among methods. Downcast and upcast salinity profiles did not have obvious dynamic errors and there were no density inversions (Fig. 16C). As such, both downcast and upcast profiles processed using the *Typical* method were selected as the best casts.

Deployment #8 sampled a two-layer stratified water column in the Western Aleutian Islands with a shallow surface mixed layer (~8 m; Fig. 17). Profiles had a sharp temperature gradient at the thermocline (Fig. 17A), which likely contributed to salinity spikes in downcasts processed using methods other than *Typical* and *Typical CTM*, and upcasts from all methods (Fig. 17B). *Typical CTM*, *TSA*, and *MSG* methods amplified dynamic errors in salinity compared to the *Typical* method and resulted in density inversions in upcasts (Fig. 17C), likely due to overcorrecting small-scale temperature and salinity variation. Based on visual inspection, the *Typical* method downcast was selected as the best cast.

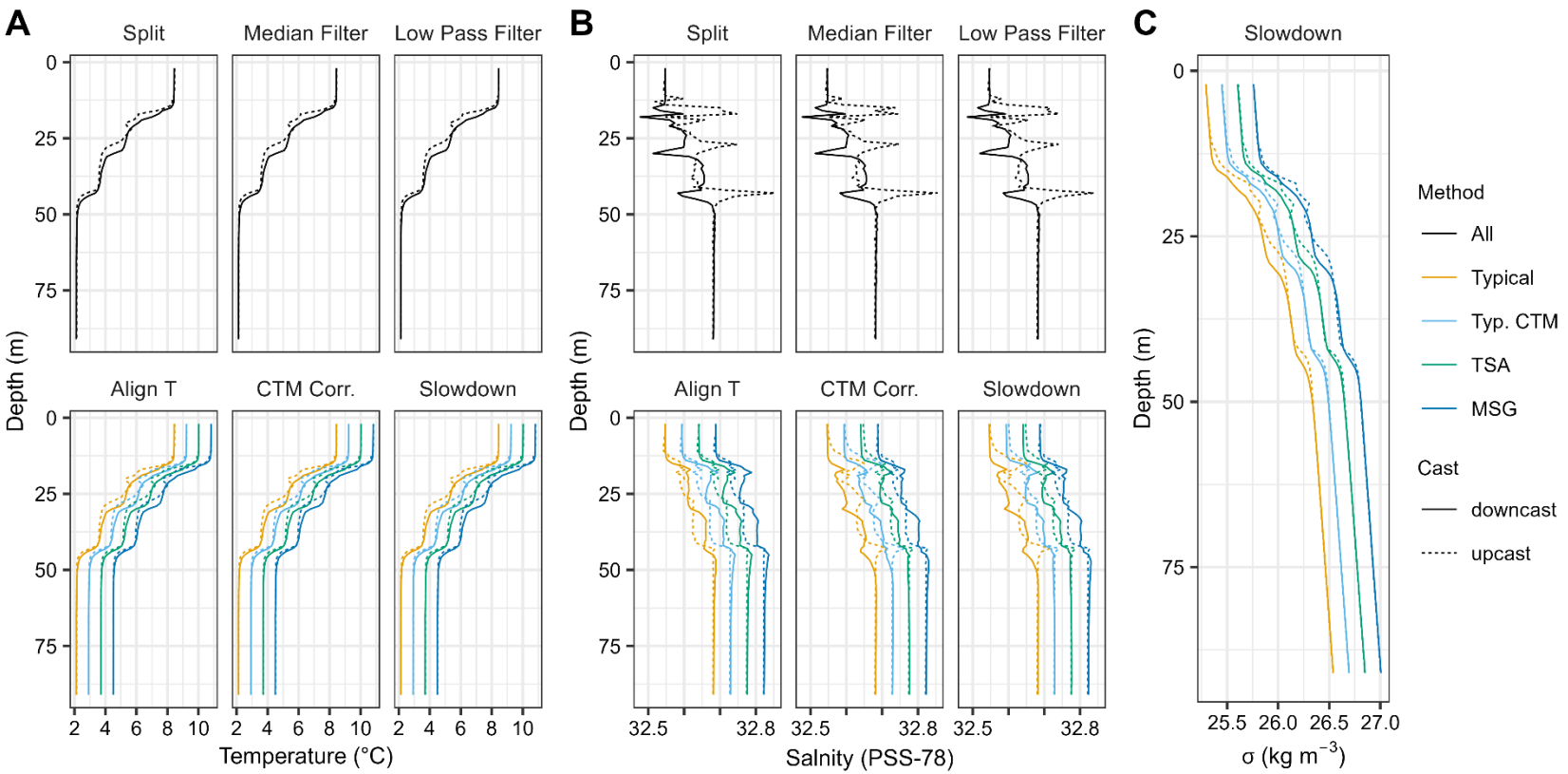


Figure 9. -- Deployment #1 profiles of (A) depth versus temperature (°C), (B) depth versus salinity (PSS-78), and (C) depth versus potential density anomaly, $\sigma_\theta$ (kg m$^{-3}$), that were processed using the four data processing methods (*Typical*, *Typical conductivity cell thermal mass correction* [*Typ. CTM*], *Temperature-Salinity Area* [*TSA*], *Minimal Salinity Gradient* [*MSG*]) at different stages of data processing. 'All' denotes steps that were common to all four processing methods. Results are shown after splitting downcasts and upcasts (Split), median filtering, low pass filtering, aligning temperature (Align T), conductivity cell thermal mass correction (CTM Corr.), and Slowdown. Temperature and salinity values are the mean for 1-m depth bins. Temperature, salinity, and $\sigma_\theta$ profiles for are offset by 12.5%, 25%, and 37.5% of temperature/salinity$\sigma_\theta$ ranges when *Typical CTM*, *TSA*, or *MSG* curves are shown to facilitate interpretability.

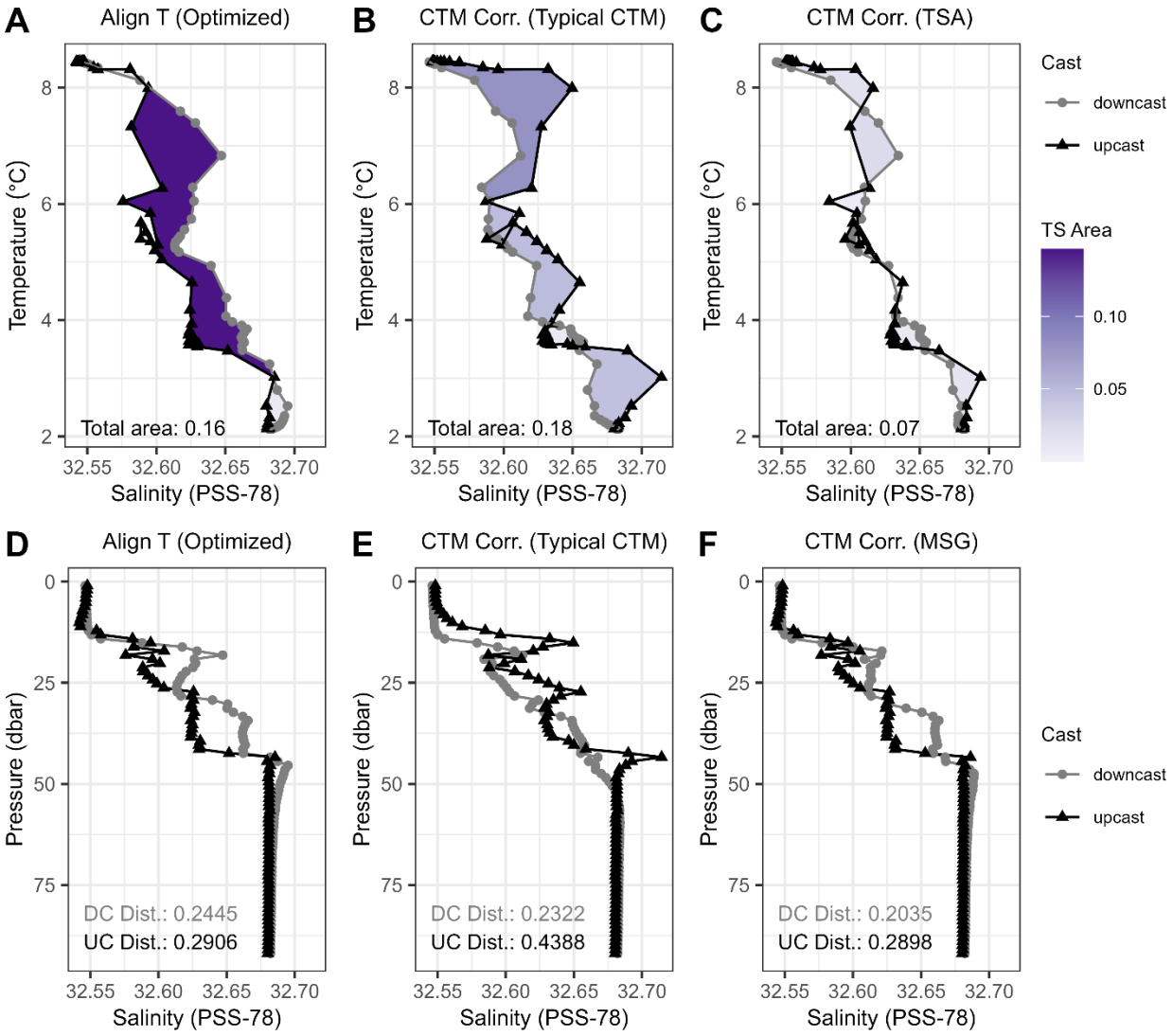


Figure 10. -- Effects of conductivity cell thermal mass correction on temperature-salinity area profiles (panels A–C) and salinity versus pressure profiles (panels D–F) for Deployment #1. Panels show profiles before conductivity cell thermal mass correction (Align T [Optimize]; A and D), after the *Typical conductivity cell thermal mass correction* method (CTM Corr [Typ.CTM]; B and E), after optimizing conductivity cell thermal mass correction parameters using the *Temperature-Salinity Area* method (CTM Corr. [TSA]; C), and after optimizing using the *Minimal Salinity Gradient* method (CTM Corr. [MSG]; F). In panels A–C, the fill color denotes the areas of individual polygons that comprise the area between downcast and upcast temperature-salinity curves and the total area is shown at the bottom left of each panel. In panels D–F, text on the bottom left of each panel shows the minimum salinity gradient for downcast (DC) and upcast (UC) salinity curves.

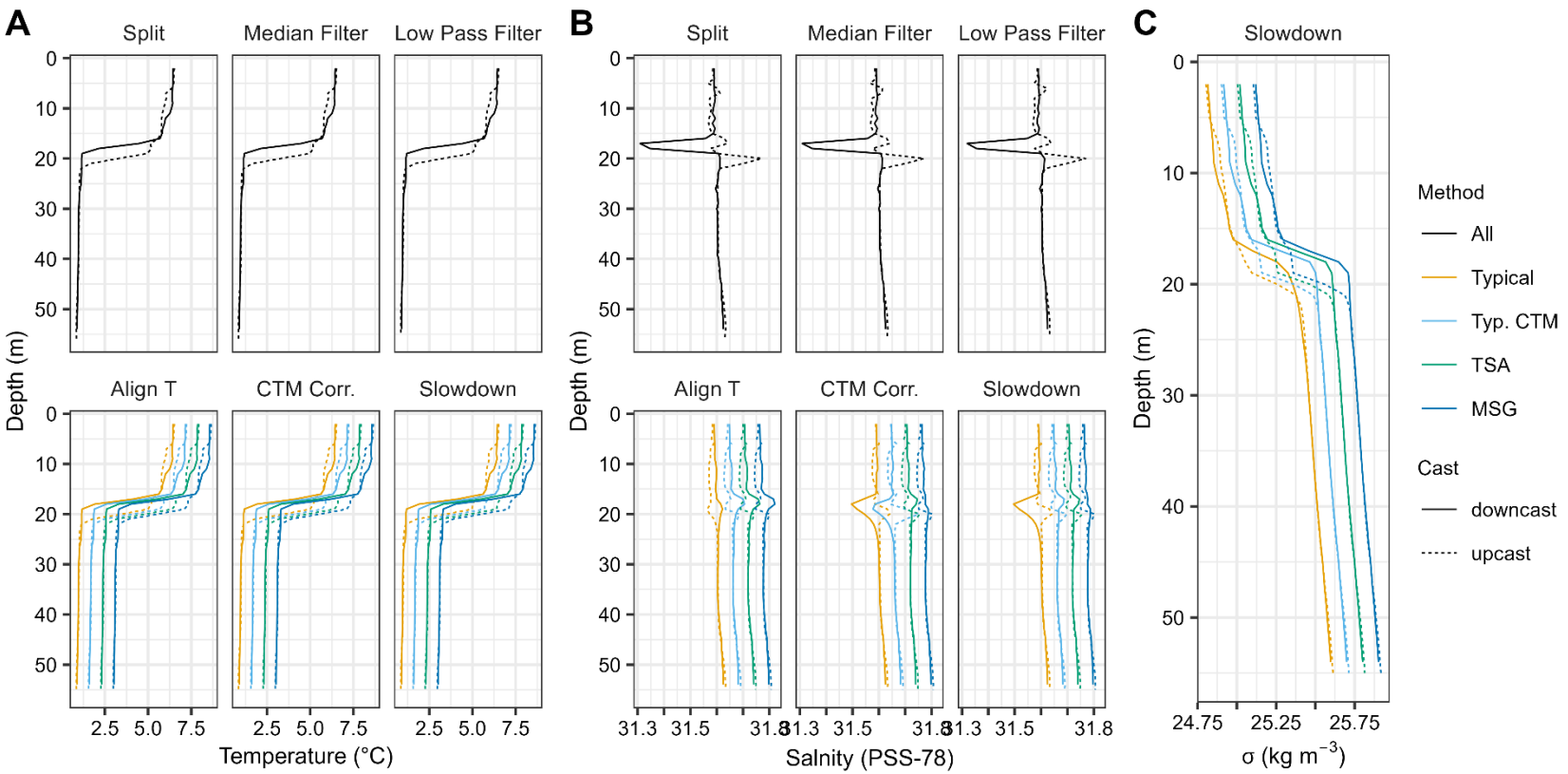


Figure 11. -- Deployment #2 profiles of (A) depth versus temperature (°C), (B) depth versus salinity (PSS-78), and (C) depth versus potential density anomaly, $\sigma_\theta$ (kg m$^{-3}$), that were processed using the four data processing methods (*Typical*, *Typical conductivity cell thermal mass correction* [*Typ. CTM*], *Temperature-Salinity Area* [*TSA*], *Minimum Salinity Gradient* [*MSG*]) at different stages of data processing. 'All' denotes steps that were common to all four processing methods. Results are shown after splitting downcasts and upcasts (Split), median filtering, low pass filtering, aligning temperature (Align T), conductivity cell thermal mass correction (CTM Corr.), and Slowdown. Temperature and salinity values are the mean for 1-m depth bins. Temperature, salinity, and $\sigma_\theta$ profiles for are offset by 12.5%, 25%, and 37.5% of temperature/salinity$\sigma_\theta$ ranges when *Typical CTM*, *TSA*, or *MSG* curves are shown to facilitate interpretability.

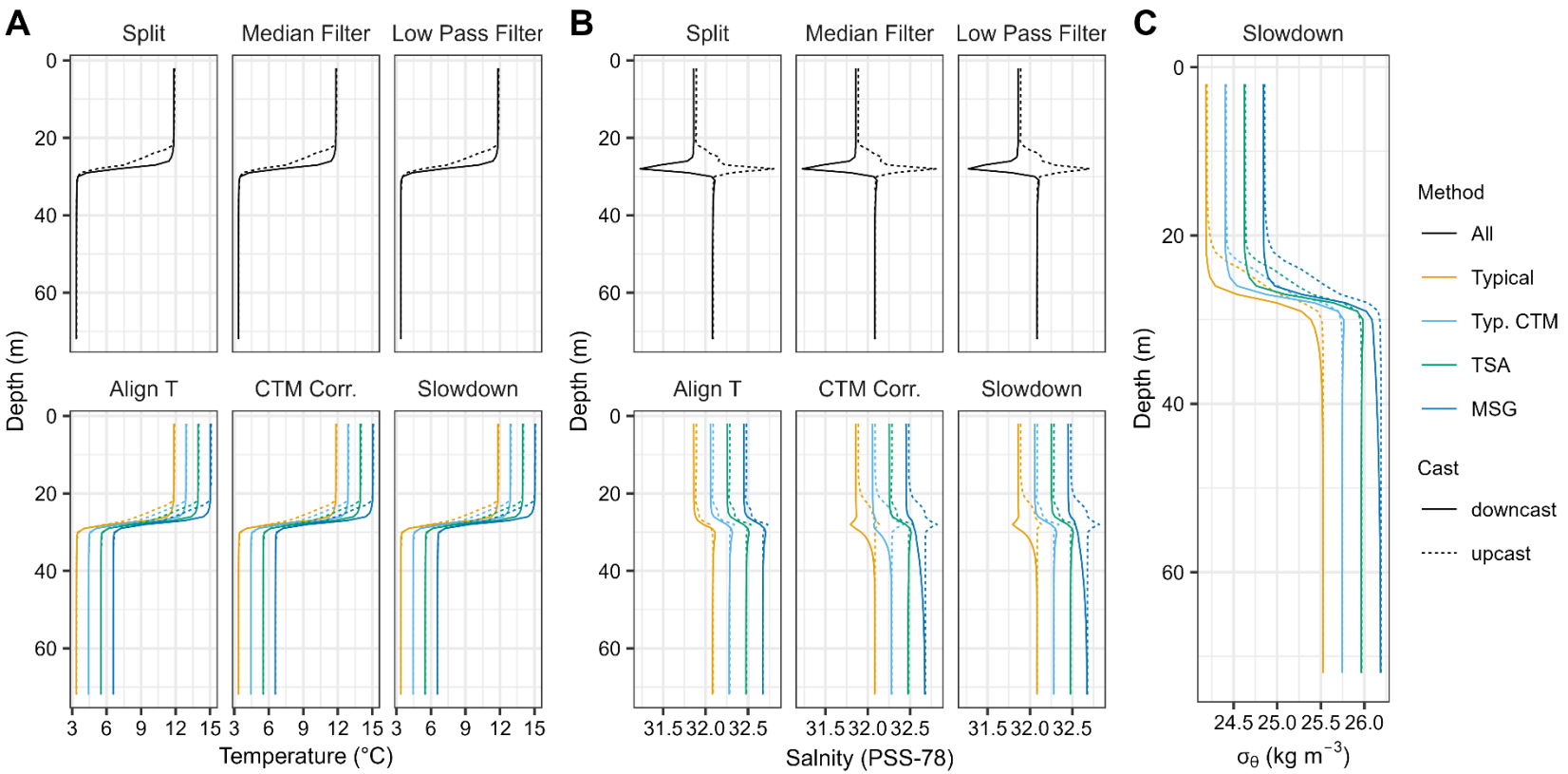


Figure 12. -- Deployment #3 profiles of (A) depth versus temperature (°C), (B) depth versus salinity (PSS-78), and (C) depth versus potential density anomaly, $\sigma_\theta$ (kg m$^{-3}$), that were processed using the four data processing methods (*Typical*, *Typical conductivity cell thermal mass correction* [*Typ. CTM*], *Temperature-Salinity Area* [*TSA*], *Minimum Salinity Gradient* [*MSG*]) at different stages of data processing. 'All' denotes steps that were common to all four processing methods. Results are shown after splitting downcasts and upcasts (Split), median filtering, low pass filtering, aligning temperature (Align T), conductivity cell thermal mass correction (CTM Corr.), and Slowdown. Temperature and salinity values are the mean for 1-m depth bins. Temperature, salinity, and $\sigma_\theta$ profiles for are offset by 12.5%, 25%, and 37.5% of temperature/salinity$\sigma_\theta$ ranges when *Typical CTM*, *TSA*, or *MSG* curves are shown to facilitate interpretability.

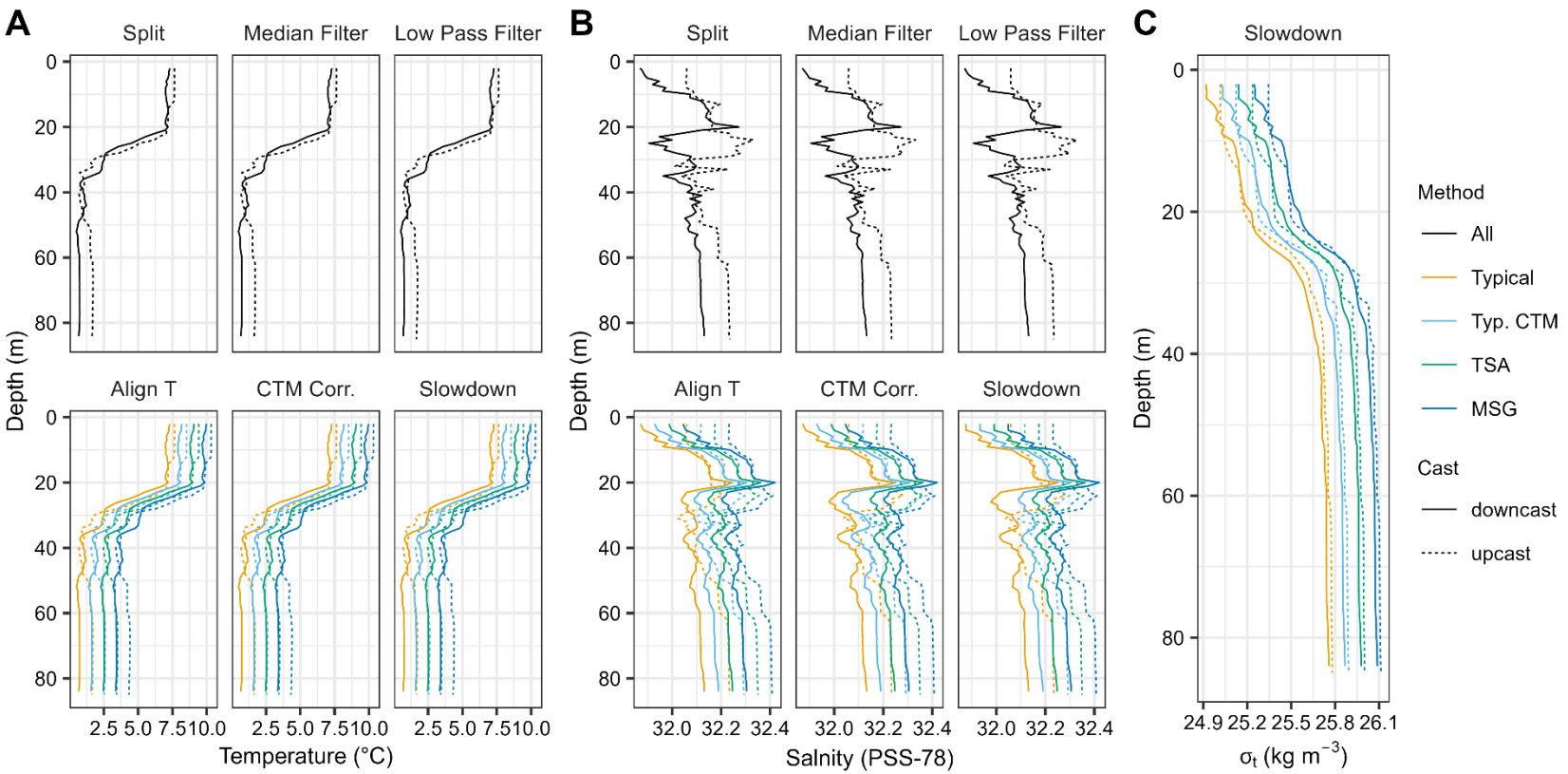


Figure 13. -- Deployment #4 profiles of (A) depth versus temperature (°C), (B) depth versus salinity (PSS-78), and (C) depth versus potential density anomaly, $\sigma_\theta$ (kg m$^{-3}$), that were processed using the four data processing methods (*Typical*, *Typical conductivity cell thermal mass correction* [*Typ. CTM*], *Temperature-Salinity Area* [*TSA*], *Minimum Salinity Gradient* [*MSG*]) at different stages of data processing. 'All' denotes steps that were common to all four processing methods. Results are shown after splitting downcasts and upcasts (Split), median filtering, low pass filtering, aligning temperature (Align T), conductivity cell thermal mass correction (CTM Corr.), and Slowdown. Temperature and salinity values are the mean for 1-m depth bins. Temperature, salinity, and $\sigma_\theta$ profiles for are offset by 12.5%, 25%, and 37.5% of temperature/salinity$\sigma_\theta$ ranges when *Typical CTM*, *TSA*, or *MSG* curves are shown to facilitate interpretability.

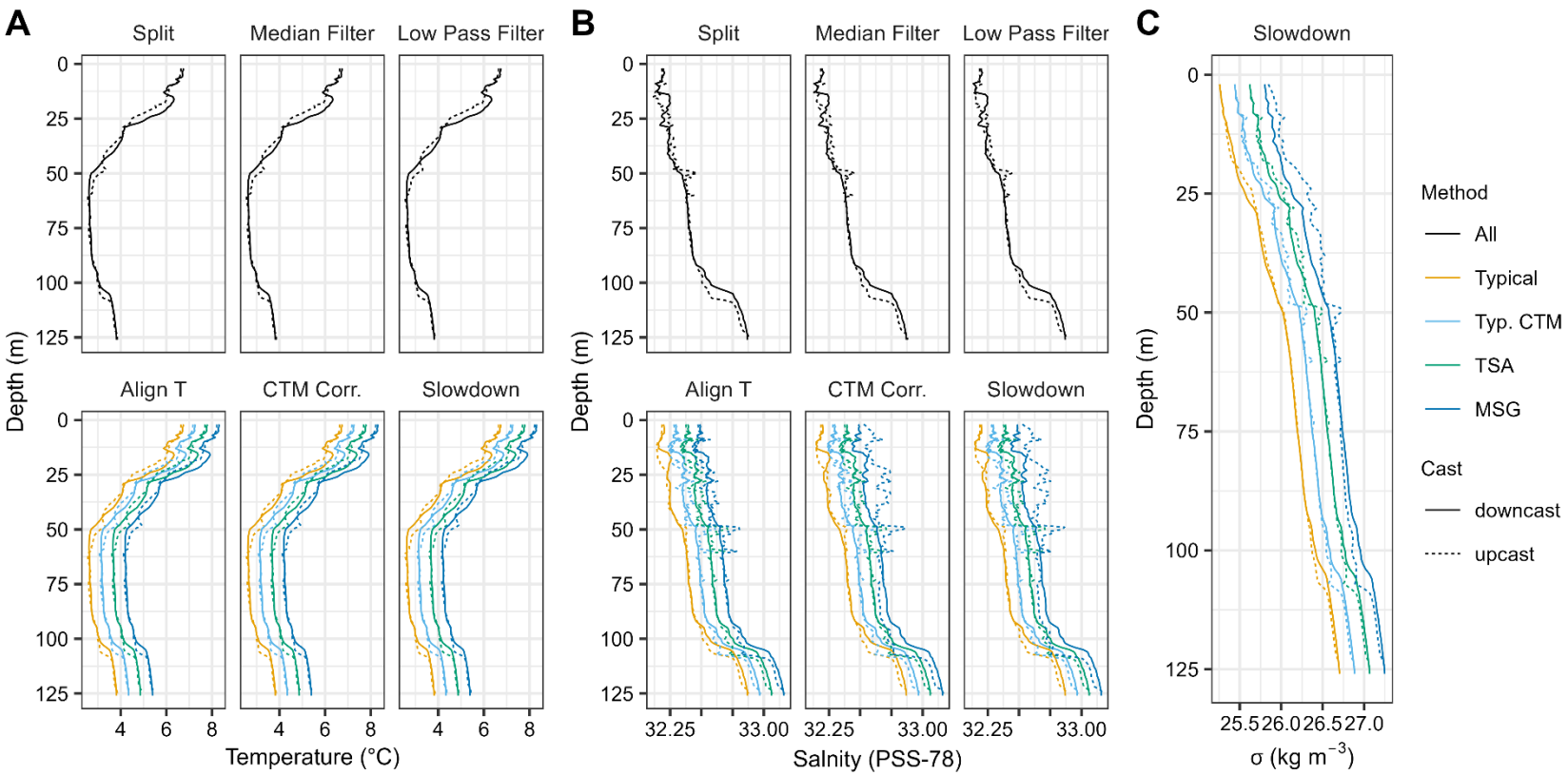


Figure 14. -- Deployment #5 profiles of (A) depth versus temperature (°C), (B) depth versus salinity (PSS-78), and (C) depth versus potential density anomaly, $\sigma_\theta$ (kg m$^{-3}$), that were processed using the four data processing methods (*Typical*, *Typical conductivity cell thermal mass correction* [*Typ. CTM*], *Temperature-Salinity Area* [*TSA*], *Minimum Salinity Gradient* [*MSG*]) at different stages of data processing. 'All' denotes steps that were common to all four processing methods. Results are shown after splitting downcasts and upcasts (Split), median filtering, low pass filtering, aligning temperature (Align T), conductivity cell thermal mass correction (CTM Corr.), and Slowdown. Temperature and salinity values are the mean for 1-m depth bins. Temperature, salinity, and $\sigma_\theta$ profiles for are offset by 12.5%, 25%, and 37.5% of temperature/salinity$\sigma_\theta$ ranges when *Typical CTM*, *TSA*, or *MSG* curves are shown to facilitate interpretability.

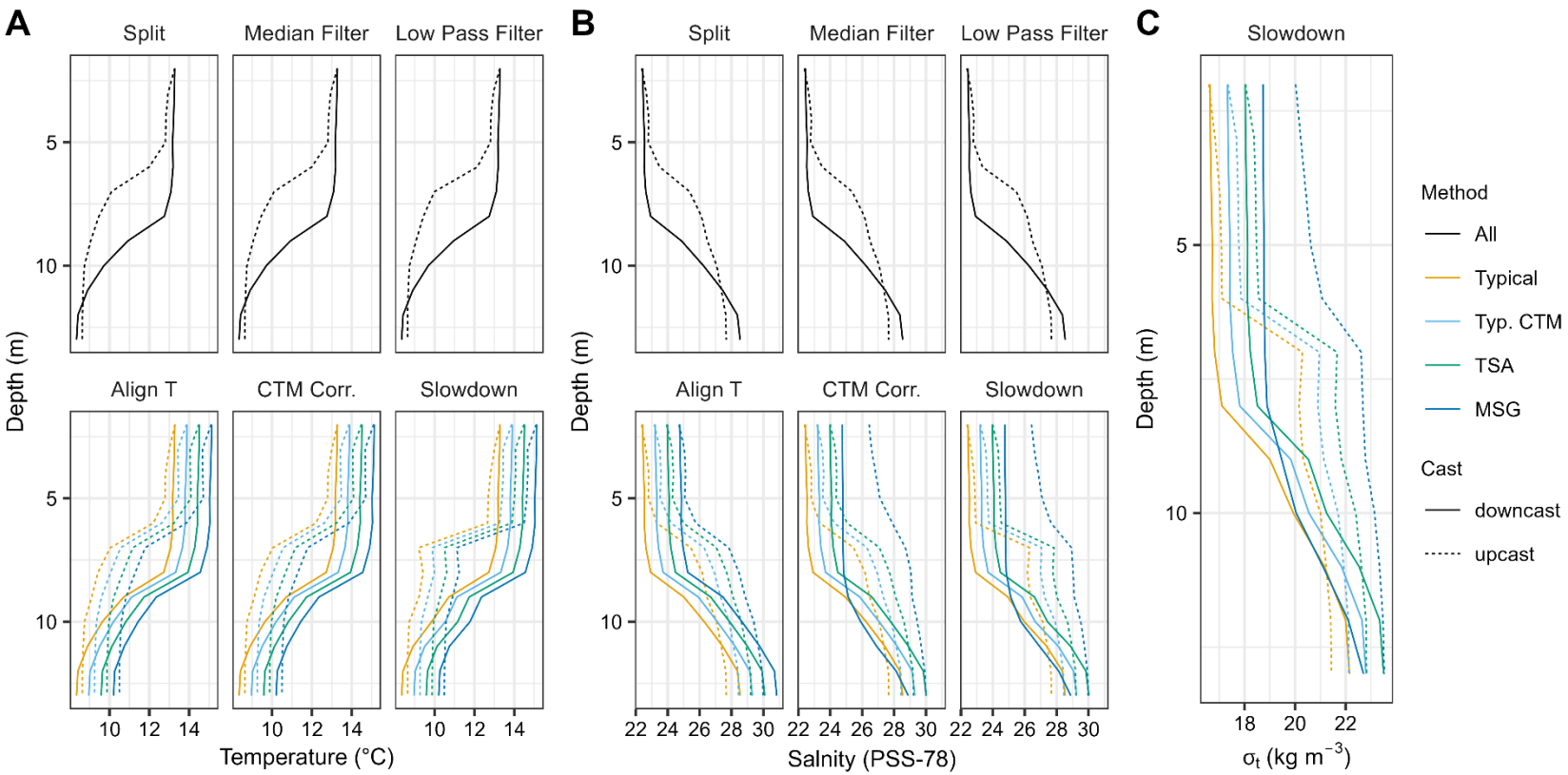


Figure 15. -- Deployment #6 profiles of (A) depth versus temperature (°C), (B) depth versus salinity (PSS-78), and (C) depth versus potential density anomaly, $\sigma_\theta$ (kg m$^{-3}$), that were processed using the four data processing methods (*Typical*, *Typical conductivity cell thermal mass correction* [*Typ. CTM*], *Temperature-Salinity Area* [*TSA*], *Minimum Salinity Gradient* [*MSG*]) at different stages of data processing. 'All' denotes steps that were common to all four processing methods. Results are shown after splitting downcasts and upcasts (Split), median filtering, low pass filtering, aligning temperature (Align T), conductivity cell thermal mass correction (CTM Corr.), and Slowdown. Temperature and salinity values are the mean for 1-m depth bins. Temperature, salinity, and $\sigma_\theta$ profiles for are offset by 12.5%, 25%, and 37.5% of temperature/salinity$\sigma_\theta$ ranges when *Typical CTM*, *TSA*, or *MSG* curves are shown to facilitate interpretability.

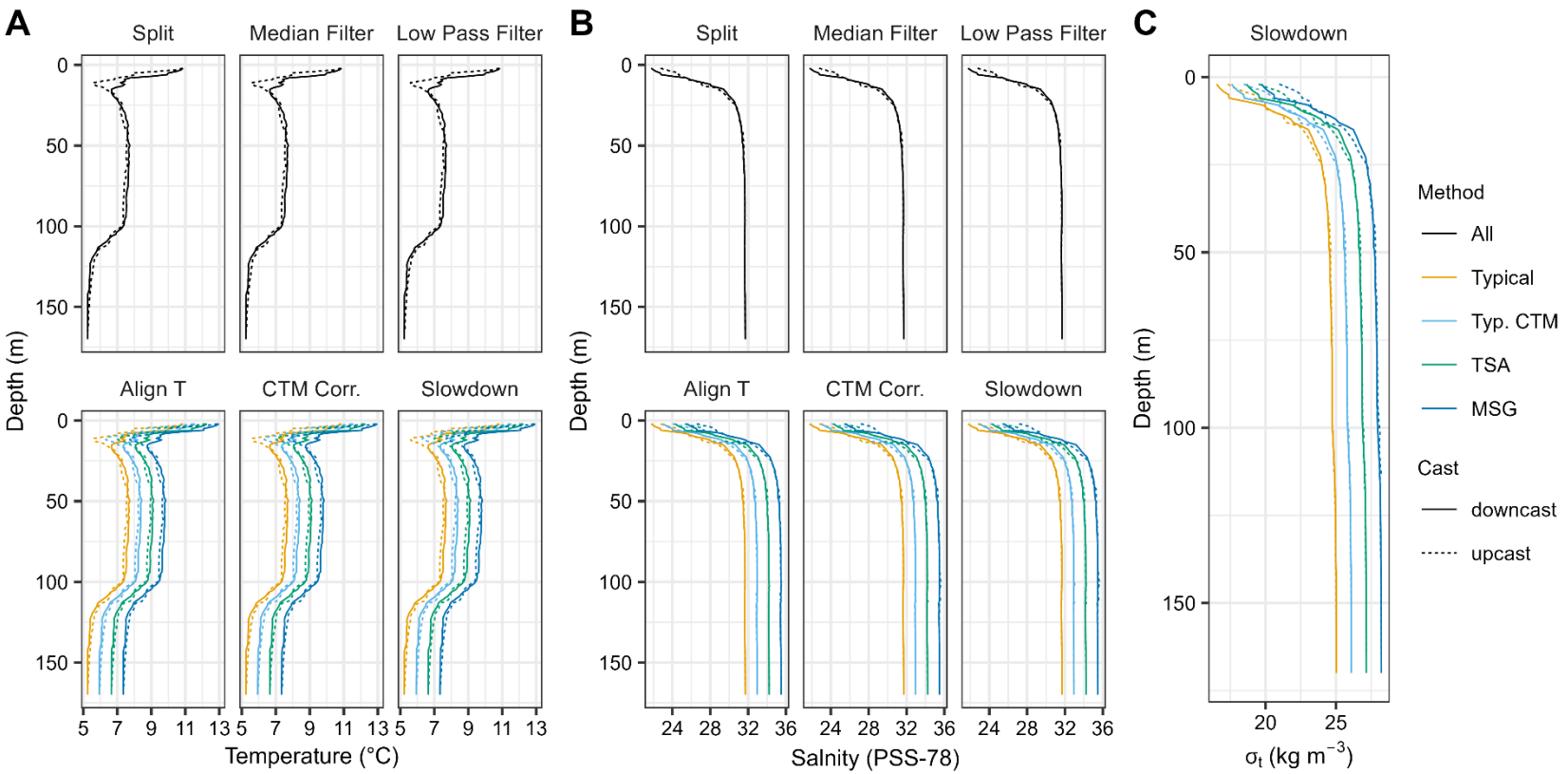


Figure 16. -- Deployment #7 profiles of (A) depth versus temperature (°C), (B) depth versus salinity (PSS-78), and (C) depth versus potential density anomaly, $\sigma_\theta$ (kg m$^{-3}$), that were processed using the four data processing methods (*Typical*, *Typical conductivity cell thermal mass correction* [*Typ. CTM*], *Temperature-Salinity Area* [*TSA*], *Minimum Salinity Gradient* [*MSG*]) at different stages of data processing. 'All' denotes steps that were common to all four processing methods. Results are shown after splitting downcasts and upcasts (Split), median filtering, low pass filtering, aligning temperature (Align T), conductivity cell thermal mass correction (CTM Corr.), and Slowdown. Temperature and salinity values are the mean for 1-m depth bins. Temperature, salinity, and $\sigma_\theta$ profiles for are offset by 12.5%, 25%, and 37.5% of temperature/salinity$\sigma_\theta$ ranges when *Typical CTM*, *TSA*, or *MSG* curves are shown to facilitate interpretability.

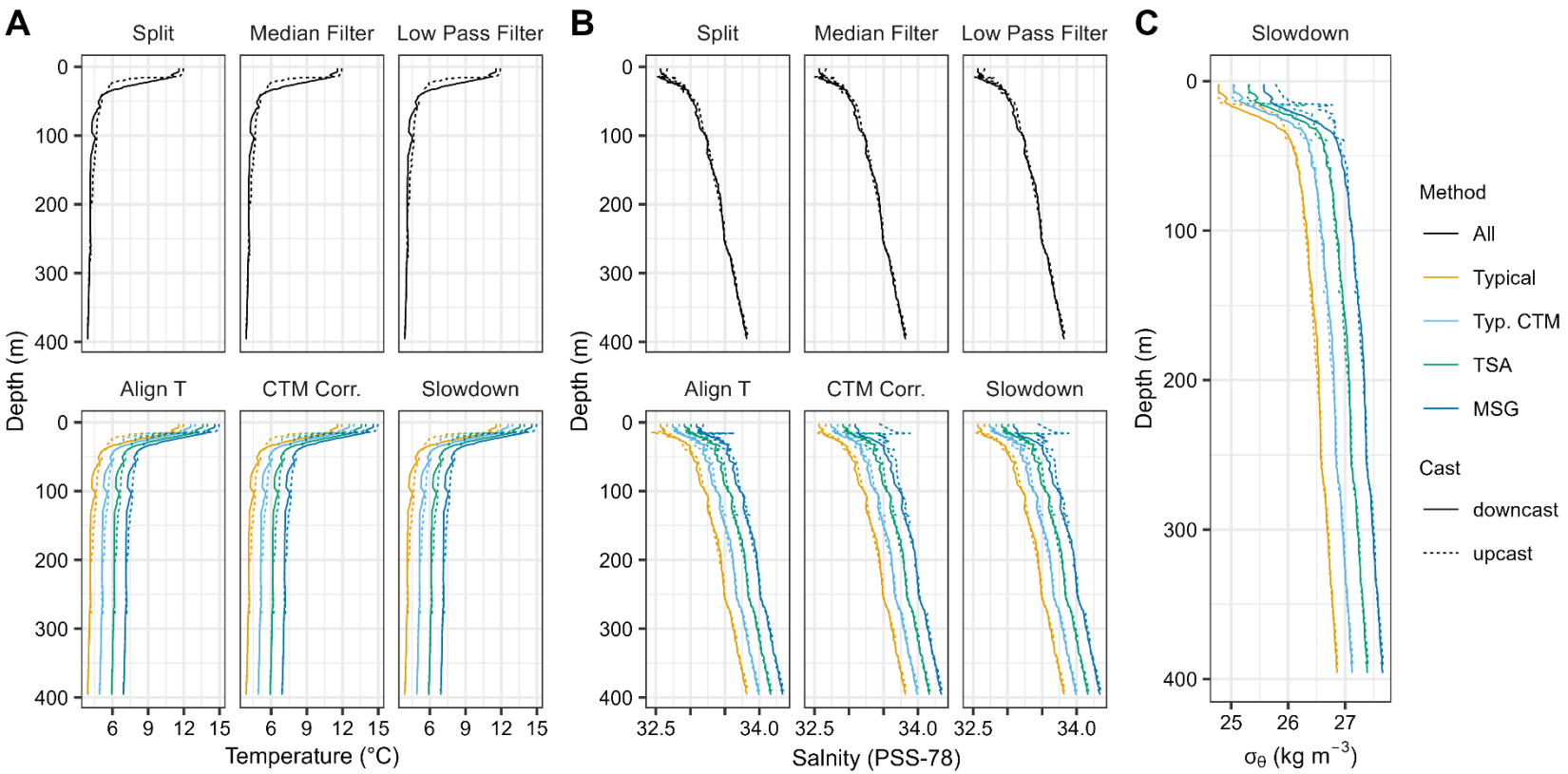


Figure 17. -- Deployment #8 profiles of (A) depth versus temperature (°C), (B) depth versus salinity (PSS-78), and (C) depth versus potential density anomaly, $\sigma_\theta$ (kg m$^{-3}$), that were processed using the four data processing methods (*Typical*, *Typical conductivity cell thermal mass correction* [*Typ. CTM*], *Temperature-Salinity Area* [*TSA*], *Minimum Salinity Gradient* [*MSG*]) at different stages of data processing. 'All' denotes steps that were common to all four processing methods. Results are shown after splitting downcasts and upcasts (Split), median filtering, low pass filtering, aligning temperature (Align T), conductivity cell thermal mass correction (CTM Corr.), and Slowdown. Temperature and salinity values are the mean for 1-m depth bins. Temperature, salinity, and $\sigma_\theta$ profiles for are offset by 12.5%, 25%, and 37.5% of temperature/salinity$\sigma_\theta$ ranges when *Typical CTM*, *TSA*, or *MSG* curves are shown to facilitate interpretability.

### Effect of trawl-mounted CTD on trawl height

There was no evidence that the CTD affected the fishing height of the trawl gear in the GOA because the 95% credible interval of the CTD effect (-0.25 to 0.07 m) in the mixed effects model included 0 m. This result does not rule out the possibility that the CTD affects the fishing height of the trawl. However, if the CTD affects trawl height, the magnitude of the effect is likely small compared to estimated differences in average fishing height among individual trawl nets (height range: 5.42 to 6.77 m; Fig. 18).

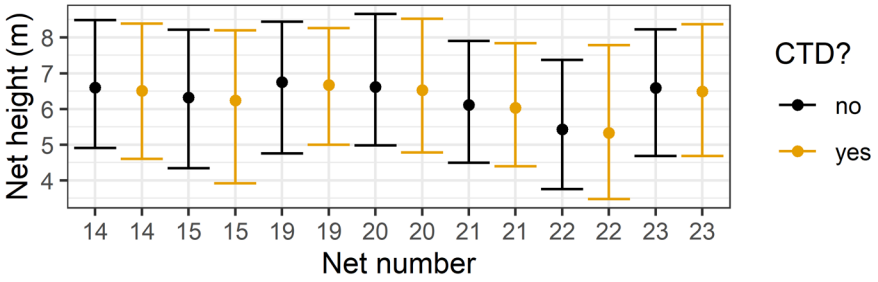


Figure 18. -- Mixed-effects model predictions of fishing height with or without the CTD deployed on the net during the 2021 Gulf of Alaska Bottom Trawl Survey. Circles denote the mean prediction, bars denote 95% credible interval, and colors denote whether predictions are for hauls with ("yes"; orange) or without ("no"; black) the CTD.

## DISCUSSION

Large dynamic errors in salinity were mitigated in at least one cast (downcast or upcast) in the majority of deployments by using our approach of processing trawl-mounted CTD data using four methods then selecting the best method for each deployment. The *Typical* method used the manufacturer's recommended typical settings for data processing modules and was selected for the majority of deployments, including ≥ 99% of deployments in the Gulf of Alaska (GOA) and Aleutian Islands (AI). However, in the eastern Bering Sea (EBS) and northern Bering Sea (NBS), methods that optimized parameters for temperature alignment or conductivity cell thermal mass correction modules (*Typical CTM*, *TSA*, *MSG*) were selected 29.1% of the time. The rates at which different methods were selected for the different regions appears to be related to regional differences in thermohaline structure of the water column, as the EBS and NBS had sharper thermocline temperature gradients than the AI

and GOA, which tended to cause erroneous salinity spikes around the thermocline. These results indicate that the optimal dynamic error correction method for trawl-mounted CTD data varies with instrument capabilities and operating conditions, similar to other CTD deployment methods (Mensah et al. 2009, Ullman and Hebert 2014).

Studies have previously reported methods for processing trawl-mounted CTD data (Van Vraken et al. 2020) for instruments with different operating characteristics than the SBE 19plus V2, but we are unaware of any that have used our method. Notably, Cokelet (2016) reported data processing methods for data collected during AFSC bottom-trawl surveys of the eastern Bering Sea and northern Bering Sea using a trawl-mounted Teledyne RD Instruments Citadel CTD-NV. However, the SBE 19plus V2 has different operating characteristics than the Citadel CTD-NV, which necessitates different data processing methods. The SBE 19plus uses a pump to maintain constant flow rates past sensors and has a sampling rate of 4 Hz with limiting sensor response of 0.5 s[2]. This contrasts with the CTD-NV that has a 15 Hz sampling rate with a limiting sensor response time of 0.1 seconds for the temperature sensor at a flow rate of 1 m $s^{-1}$. Although the SBE 19plus V2 has a slower sampling frequency than the Citadel CTD-NV, the pump reduces the effect of variable profiling speeds on sensor response times.

The optimal temperature alignment can vary with profiling rate in towed CTD data (Ullman and Hebert, 2014), but we did not find a meaningful relationship between profiling rate and optimal temperature alignment in our trawl-mounted CTD data. This is not surprising because the CTDs were equipped with pumps, which helps maintain a constant flow rate past sensors that help to promote a consistent lag in temperature relative to pressure. This contrasts with unpumped towed CTDs, where changes in descent and ascent rates lead to variable flow rates past sensors. However, estimated temperature alignment offset parameters often differed from recommended typical value (temperature-lagged 0.5 s relative to pressure) and there was a mode in temperature alignment offset, $t_T$, at -1.0 s. We cannot determine what causes variation in the temperature alignment offset using our data, but variation in the physical alignment of the CTD housing within the mesh bag among hauls or in flow dynamics around the CTD may play a role.

Profiling speeds were usually slower than those recommended by the manufacturer (0.5 to 2.0 m $s^{-1}$) but data quality appeared reasonable, potentially because trawl gear dampens effects of ship heave. Examining the effects of waves on the height and bottom contact of the 83-112 bottom gear used for EBS shelf and NBS surveys, Somerton et al. (2018) found that the period of oscillations in trawl

[2] Sea-Bird Scientific. (2017, July). Application Note 98: Considerations for CTD Spatial and Temporal Resolutions on Moving Platforms. https://www.seabird.com/asset-get.download.jsa?id=54627861734. Accessed 25 May 2022.

components matched the period of oscillations in ship heave, showing that wave and vessel motion are transferred to the trawl gear. However, the amplitude of oscillations in trawl components (~1–6 cm) was 1–2 orders of magnitude smaller than the amplitude of ship-heave, which, in turn, was around an order of magnitude smaller than wave amplitude. Although Somerton et al. (2018) focused on the configuration of the net while it was on-bottom, their results highlight that trawl gear dampens ship heave, which likely reduces the impact of slowdowns and reversals compared to winch-based deployments.

Our data processing method will be useful for producing operational CTD data products immediately after the conclusion of AFSC RACE GAP's annual summer bottom-trawl surveys. Environmental data collected during AFSC RACE GAP summer bottom-trawl surveys using temperature-depth recorders are already used calculate indicators of ecosystem conditions in support of ecosystem-based fisheries management (e.g., Rohan et al. 2022). The indicators are also used as covariates in stock assessment models and individual data are used to characterize species-environment relationships using species distribution models to support delineation of Essential Fish Habitat (Laman et al. 2018). CTD data could similarly be used as a basis to produce ecosystem indicators. However, to provide 'operational' information during the same year as the surveys, data must be processed and indicators must be derived between the end of the summer surveys (late July to mid-August) and the deadlines for groundfish stock assessment and reports to management (August to October, depending on the application). Using efficient and consistent data processing methods is essential for meeting operational timelines and ensuring that results are comparable among years.

## ACKNOWLEDGMENTS

We thank Victor Simon and Sean Rooney for input on the deployment and maintenance of CTDs, Wayne Palsson for initial project coordination, and Shawn Russell and the AFSC Net Loft team for setting up trawl gear for CTD deployments. We are extremely grateful to Ned Cokelet, Chris Melrose, and Duane Stevenson for providing constructive reviews that greatly improved the quality of this manuscript. We thank the vessel captains, crews, and survey personnel who helped collect the data at sea.

## CITATIONS


Arimitsu, M. L., Piatt, J. F., and Mueter, F. 2016. Influence of glacier runoff on ecosystem structure in Gulf of Alaska fjords. Marine Ecology Progress Series 560: 19–40. https://doi.org/10.3354/meps11888

Barth, J. A., O'Malley, R. T., Fleischbein, J., Smith, R. L., and Huyer, A. 1996. SeaSoar and CTD observations during coastal jet separation cruise W9408A, August to September 1994. Oregon State University, College of Oceanic and Atmospheric Sciences Technical Report. 162, 170 p. https://ir.library.oregonstate.edu/concern/defaults/fj236371s

Byrd, R. H., Lu, P., Nocedal, J., and Zhu, C. 1995. A limited memory algorithm for bound constrained optimization. SIAM Journal on Scientific Computing 16: 1190–1208. https://doi.org/10.1137/0916069

Cokelet, E. D. 2016. 3-D water properties and geostrophic circulation on the eastern Bering Sea shelf. Deep Sea Research Part II: Topical Studies in Oceanography 134: 65–85. https://doi.org/10.1016/j.dsr2.2016.08.009

Dever, M., Freilich, M., Farrar, J. T., Hodges, B., Lanagan, T., Baron, A. J., and Mahadevan, A. 2020. EcoCTD for profiling oceanic physical–biological properties from an underway ship. Journal of Atmospheric and Oceanic Technology 37(5): 825–840. https://doi.org/10.1175/JTECH-D-19-0145.1

Garau, B., Ruiz, S., Zhang, W. G., Pascual, A., Heslop, E., Kerfoot, J., and Tintoré, J. 2011. Thermal lag correction on Slocum CTD glider data. Journal of Atmospheric and Oceanic Technology 28(9): 1065–1071. https://doi.org/10.1175/JTECH-D-10-05030.1

Goodrich, B., Gabry, J., Ali, I., and Brilleman, S. 2022. rstanarm: Bayesian applied regression modeling via Stan. R package version 2.21.3. https://mc-stan.org/rstanarm

Harris, J., Pirtle, J., Laman, E. A., Siple, M. C. and Thorson, J. T. In review. Ensemble models mitigate bias in habitat utilization and range area from commonly used species distribution models.

Kearney, K. A. 2019. Freshwater input to the Bering Sea, 1950–2017. U.S. Department of Commerce, NOAA Technical Memorandum NMFS-AFSC-388, 46 p. https://doi.org/10.25923/vcj6-h740

Kelley, D., and Richards, C. 2022. *oce*: *Analysis of oceanographic data.* R Package version 1.7-10. https://cran.r-project.org/package=oce

Kelley, D., Richards, C., and Layton, C. 2022. oce: An R package for oceanographic analysis. Journal of Open Source Software 7(71): 3594. https://doi.org/10.21105/joss.03594

Laman, E. A., Rooper, C. N., Turner, K., Rooney, S., Cooper, D. W., and Zimmermann, M. 2018. Using species distribution models to describe essential fish habitat in Alaska. Canadian Journal of Fisheries and Aquatic Sciences. 75(8): 1230–1255. https://doi.org/10.1139/cjfas-2017-0181

Lauth, R. R., and Kotwicki, S. 2014. A calibration function for correcting mean net spread values obtained from Marport spread sensors used in conjunction with the Marport MK II receiver. AFSC Processed Rep. 2014-02, 26 p. Alaska Fish. Sci. Cent., NOAA, Natl. Mar. Fish. Serv., 7600 Sand Point Way NE, Seattle WA 98115.

Lueck, R. G., and Picklo, J. J. 1990. Thermal inertia of conductivity cells: observations with a sea-bird cell. Journal of Atmospheric and Oceanic Technology 7(5): 756–768. https://doi.org/10.1175/1520-0426(1990)007<0756:TIOCCO>2.0.CO;2

Markowitz, E. H., Dawson, E. J., Charriere, N. E., Prohaska, B. K., Rohan, S. K., Stevenson, D. E., and Britt, L. L. 2022. Results of the 2021 eastern and northern Bering Sea continental shelf bottom trawl survey of groundfish and invertebrate fauna. U.S. Department of Commerce, NOAA Technical Memorandum NMFS-AFSC-452, 227 p. https://doi.org/10.25923/g1ny-y360

Martini, K. I., Murphy, D. J., Schmitt, R. W., and Larson, N. G. 2019. Corrections for pumped SBE 41CP CTDs determined from stratified tank experiments. Journal of Atmospheric and Oceanic Technology 36(4): 733–744. https://doi.org/10.1175/JTECH-D-18-0050.1

Mensah, V., Le Menn, M., and Morel, Y. 2009. Thermal mass correction for the evaluation of salinity. Journal of Atmospheric and Oceanic Technology 26(3): 665–672. https://doi.org/10.1175/2008JTECHO612.1

Morison, J., Andersen, R., Larson, N., D'Asaro, E., and Boyd, T. 1994. The correction for thermal-lag effects in Sea-Bird CTD data. Journal of Atmospheric and Oceanic Technology 11(4): 1151–1164. https://doi.org/10.1175/1520-0426(1994)011<1151:TCFTLE>2.0.CO;2

Rohan, S. K., Barnett, L. A. K., and Charriere, N. 2022. Evaluating approaches to estimating mean temperatures and cold pool area from AFSC bottom trawl surveys of the eastern Bering Sea. U.S. Department of Commerce, NOAA Technical Memorandum NMFS-AFSC-456, 42 p. https://doi.org/10.25923/1wwh-q418

Somerton, D. A., and Munro, P. 2001. Bridle efficiency of a survey trawl for flatfish. Fishery Bulletin, U.S. 99(4): 641–652.

Somerton, D., Weinberg, K., Munro, P., Rugolo, L., and Wilderbuer, T. 2018. The effects of wave-induced vessel motion on the geometry of a bottom survey trawl and the herding of yellowfin sole (*Limanda aspera*). Fishery Bulletin, U.S. 116(1): 21–33. https://doi.org/10.7755/FB.116.1.3

Ullman, D. S., and Hebert, D. 2014. Processing of underway CTD data. Journal of Atmospheric and Oceanic Technology 31(4): 984–998. https://doi.org/10.1175/JTECH-D-13-00200.1

Van Vranken, C., Vastenhoud, B. M. J., Manning, J. P., Plet-Hansen, K. S., Jakoboski, J., Gorringe, P., and Martinelli, M. 2020. Fishing gear as a data collection platform: Opportunities to fill spatial and temporal gaps in operational sub-surface observation networks. Frontiers in Marine Science *7*. https://doi.org/10.3389/fmars.2020.485512

von Szalay, P. G., and Raring, N. W. 2020. Data Report: 2018 Aleutian Islands bottom trawl survey. U.S. Department of Commerce, NOAA Technical Memorandum NMFS-AFSC-409, 175 p. https://doi.org/10.25923/qe5v-fz70


U.S. Secretary of Commerce
Gina M. Raimondo

Under Secretary of Commerce for Oceans and Atmosphere
Dr. Richard W. Spinrad

Assistant Administrator, National Marine Fisheries Service.
Janet Coit

September 2023

www.nmfs.noaa.gov

OFFICIAL BUSINESS

National Marine Fisheries Service
Alaska Fisheries Science Center
7600 Sand Point Way N.E.
Seattle, WA 98115-6349